

Response to comments on “A global map of emission clumps for future monitoring of fossil fuel CO₂ emissions from space” by Y. Wang et al.

We thank the referee for reviewing our manuscript. Please find attached a point-by point reply (in black) to each of the comments raised by the referee (in blue) with legible text and figures organized along the text. For your convenience, changes in the revised manuscript are highlighted with dark red. All the pages and line numbers correspond to the original version of text.

This study aims at delineating areas that can generate detectable atmospheric satellite CO₂ plumes. A large fraction of fossil fuel CO₂ emissions is coming from a very small fraction of the land surface, namely the emission clumps. Identifying these clumps is important for comparing fossil fuel CO₂ emissions across different emission inventories and useful for observations of CO₂ plumes from the space. To identify the clumps, the authors developed a random walker algorithm to consider the area in the vicinity of the cores and split the area between different clumps based on the spatial gradients in the emission field. In addition, a state-of-the-art CO₂ emission inventory (ODIAC 2017) at a 30 x 30 arc-seconds is employed to perform this study. This question is interesting. However, there is a question which is not answered by the authors. As pointed out by the authors, the emission clumps could be a useful tool to “provide a global dataset of fossil fuel CO₂ emission clumps for high-resolution atmospheric inversions that will use XCO₂ imager data”. However, these emission clumps are not fixed over time. The authors should explain how their emission clumps can be used in identifying hotspots in the future global satellite imagery of XCO₂, when the emission clumps are evolving themselves from month to month and from year to year. In addition, there are some necessary information that are missed in the paper. Please see some comments below. The paper can be accepted for publication after addressing all these comments.

Response:

We would like to thank the referee for the valuable comments and suggestions for improving our manuscript.

The specific concern raised by the reviewer about the temporal variation in the emission spatial distribution and thus the identification of clumps are discussed in the reply to Comment 7 and 8. The clump map derived in this paper is based on ODIAC for the year 2016, and it could be updated annually once new versions, either from ODIAC or other high-resolution emission inventories, become available. The purpose of the study was to propose and test a new algorithm to determine clumps and to provide the global clump map for a typical year, not to analyze trends in clumps, which could be a topic for a follow up study.

Specific comments:

1) Line 21: For “cities and power plants”, the relationship between the two concepts is ambiguous.

Response:

“City” emission refers to emission other than those from power plants. Oda et al. (2018) separated the emissions from power plants (called point sources in ODIAC) and other

emissions (called non-point sources in ODIAC). The non-point sources were distributed in proportion to the nighttime light that is observed from space. To clarify the relationship between “cities” and “power plants”, we revise the sentence into: “A large fraction of fossil fuel CO₂ emissions occur within “hotspots”, such as cities (where direct CO₂ emissions related to fossil fuel combustion in transport, residential, commercial sectors, etc., excluding emissions from electricity-producing power plants, occur), isolated power plants, and manufacturing facilities, which cover a very small fraction of the land surface...”

2) Line 23: Delete “very”. I do not understand “closely”. Rephrase “there is no detailed emission inventory for most of them”. The English is not clear at some places, may be polished by a native speaker.

Response:

We delete “very”.

We revised this sentence: “...small fraction of the land surface. The coverage of all high-emitting cities and point sources across the globe by bottom-up inventories is far from complete, and for most of those covered, the uncertainties in CO₂ emission estimates in bottom-up inventories are too large to allow continuous and rigorous assessment of emission changes (Gurney et al., 2019). Spaceborne imagery of...”

We have requested several fluent English speakers to take more active roles in proofreading the whole manuscript. We hope the revised manuscript could satisfy your concerns.

3) Line 27: Define “XCO₂” before it is formally used.

Response:

We revise the sentence: “The proposed space-borne imagers with global coverage planned for the coming decade have a pixel size on the order of a few square kilometers, and an accuracy and precision of <1 ppm for individual measurements of vertically integrated columns of dry air mole fractions of CO₂ (XCO₂).”

4) Line 30: This sentence is too long, and should shorten for clarity.

Response:

We revise the sentence: “In this study, we ~~address the question of the global characterization of~~ characterize area and point fossil fuel CO₂ emitting sources (~~those hotspots are called emission clumps hereafter~~) that may cause generating coherent XCO₂ plumes ~~in~~ that may be observed from space-borne CO₂ images across the globe. We characterize these emitting sources around the globe and they are referred to as “emission clumps” hereafter. An algorithm is proposed...”

5) Line 49: For “cities and power plants”, the relationship between the two concepts is ambiguous. They may overlap.

Response:

We revise the sentence: “The contribution from cities (excluding electricity-related emissions from large power plants, see Sect. 2) and power plants to national and global mitigation efforts is thus critical (Creutzig et al., 2015; Shan et al., 2018).”

6) Line 51: This sentence is too long, and should shorten for clarity.

Response:

We revise the sentence: “The technique called atmospheric CO₂ inversion quantifies emissions based on a prior estimate from inventories, atmospheric CO₂ measurements and atmospheric transport models. Inversions of fossil fuel CO₂ emissions have...”

7) Line 82: “a high resolution global map of fossil fuel CO₂”, it seems that the authors realized the importance of a high spatial resolution. However, what about the high temporal resolution? Does this affect the identification of emission clumps?

Response:

We are aware of that there are some day-to-day and month-to-month variations in the spatial distribution of fossil fuel CO₂ emissions. And these variations can lead to variations in the spatial extent of the clump over the same timescales. In this study, we arbitrarily choose threshold-2 to be an order of magnitude smaller than threshold-1 to include marginal areas. We assume that our conservative definition of threshold-2 ensures that the effective clumps (clump cores) always stay between our boundaries, and it also ensures the consistency of the unit for which the satellite observations could provide emission estimates through one year.

In addition, in the regions experiencing fast urbanization, we agree that the clump definition should be updated annually based on the latest inventories at high resolution to track the trends in growing cities.

To address the reviewer’s concern, we revise the manuscript by:

- Adding in Line 162: “...For calculating clumps based on morning emissions, we multiplied the annual mean emission rate (unit: g C m⁻² hr⁻¹) in each grid cell of ODIAC by the average scaling factors of emissions between 6:00-12:00 local time. The day-to-day and month-to-month variations in the spatial distribution of fossil fuel CO₂ emissions may lead to temporal variations in the spatial extent of the clumps. In this study, we define the clumps based on two thresholds (see Sect. 2.2) to ensure that the effective clumps are always within the boundaries of the clumps, and that the satellite observation should provide emission estimates consistently within a year. We thus ignore the month-to-month and day-to-day variations in the emissions.”
- Adding in L422: “... In this study, threshold-2 is chosen an order of magnitude smaller than threshold-1. This choice is somewhat arbitrary to include some marginal areas. Such marginal area accounts for the fact that the outskirts of the cities could also contribute to the city cores. In addition, the marginal area ensures that the effective clumps (e.g. the cores of the clumps) will always be accounted for in the clump map within a short time span (typically within one year to among few years). With this default choice of threshold-2, ...”
- Adding in Line 447: “..., these results highlight the necessity to objectively associate the observed CO₂ plumes with underlying emitting regions. In this study, the clumps are only defined based on the ODIAC emission map for the year 2016. However, in the regions experiencing fast urbanization rates, the spatial distribution of emissions are also changing rapidly. In order to build an operational observing system in the near future, it is also necessary to consistently update the clump definition based to latest

emission maps to track the trends in the emissions and CO₂ plumes for growing cities.”

8) Line 131: Provide evidence that the emission spatial distributions do not change significantly from year to year.

Response:

We are aware that some significant spatial distribution changes may be expected for countries with fast urbanization, e.g. China and East Asia (Frolking et al., 2013). As discussed in the response to Q7, our algorithm include some marginal areas around the city cores, ensuring that the clump map always capture the effective clumps in a short period (within one year to few years). In addition, the algorithm can be applied for each year to track the year-to-year variations in the clump definition for growing cities.

We add in L131: “... We chose the year 2016 assuming that the emission spatial distributions do not change significantly from year to year. In regions with rapid urbanization rates, the emission spatial distributions may change rapidly. The analysis of such changes is out of the scope of this paper, but the clump definition can be updated consistently with the latest high-resolution emission maps for each year, using the approach presented in Sect. 2.2. The ODIAC dataset provides...”

9) Line 139-163: These two paragraphs are given under a section namely “ODIAC fossil fuel CO₂ emission map”. However, the authors are not introducing the ODIAC product here, and it confuses me a lot when I was reading these paragraphs. I cannot understand the relationship between the ODIAC product and LEO, OCO-2, GOSAT and GeoCARB imagers.

Response:

The ODIAC map provides the emission field at a high spatial resolution. However, ODIAC has a monthly temporal resolution. Because the planned LEO satellite imagers fly over a city at a local time close to noon, the plumes that impact the XCO₂ imagery are generated by morning emissions. To correctly link the XCO₂ observations and underlying emissions, morning emissions rather than the monthly mean emissions are needed. In this case, we apply the hourly profiles from TIMES to estimate the morning emissions from the monthly means. The overpass time of considered satellites determines how the ODIAC product is used.

To remove the ambiguity identified by the reviewer, we revise the manuscript by:

- Changing the title of section to “2.1 Development of a high resolution emission map of morning emissions”.
- Moving the paragraph L139-L147 into the introduction L116: “Because CO₂ produced by emissions is quickly dispersed by transport, XCO₂ plumes sampled at a given time by a satellite image usually relate to emissions that occurred few hours before its acquisition (Broquet et al., 2018). In this study, we focus on planned LEO imagers on Sentinel missions, assuming an equator crossing time around 11:30 local time (Buchwitz et al., 2013; Broquet et al., 2018) so that XCO₂ plumes sampled by these imagers are from morning emissions. Different overpass times are also possible for other satellites. For example, Equator crossing times of OCO-2 and GOSAT are 13:00-13:30 local time. Geostationary imagers may provide a better temporal coverage of the emissions; e.g. GeoCARB images are considered to sample a city for multiple times within a day

(O'Brien et al., 2016).”

- Deleting Line 146: “~~We adopt here a focus on planned Sentinel LEO imagers, and thus use annual average of morning emissions for calculating emission clumps.~~ To estimate morning emissions, ...”

10) Figure 1: I do not quite understand this graph. How do the authors divide the total cumulative share of global annual emissions into power plants and area sources?

Response:

ODIAC emissions can be provided in several emission types, such as point source (power plant) and non-point sources. The locations and emissions for power plants in ODIAC are derived from the CARDA dataset, while the area emissions are computed by distributing the national emissions other than power plants based on the nighttime light.

Fig. 1 is plotted based on such separation of emissions from power plants and area sources. The cumulative share of the area emissions are shown in blue shade, and the cumulative share of the emissions from power plants are plotted in red shade and on top of the share of area emissions.

We add in line 165: “In ODIAC, the point sources only refer to power plants in the CARMA database. ~~So in this study, we refer to sources other than power plants as area sources.~~ Before clumps are calculated, ...”

11) Line 176-216: The presentation of the method used to identify the emission clumps is not clear. I tried to follow the steps in these paragraphs, but I was stopped by “Firstly”(line177), “Secondly”(line184), “1”(line191), “2”(line196), “3”(line204), “4”(line211). The structure is unclear. Since the core of this paper is to present a new method, the authors need to convince us that this method could be easily performed and possibly repeated by other researchers.

Response:

Figures 2 and 3 may be used for a further understanding of the algorithm. “Firstly, ...” corresponds to the selection of the power plants. “Secondly, ...” corresponds to the computation of area clumps. The computation of area clumps follows four steps numbered 1) to 4).

To make it clearer, we add in line 176 “... Fig. 3 illustrates how it operates for a small domain as an example. ~~Two categories of emission clumps are defined. A) Firstly ... B) Secondly...~~ The four steps to compute area sources emission clumps are detailed as below.” In addition, we provide the code with detailed comments for the algorithm.

12) Line 176-216: Meanwhile, the authors should publish the original code that is used to produce the emission clumps.

Response:

We do provide the code, with detailed comments, that is used to produce the emission clumps.

13) Line 196: What is the relationship between the emission clumps identified by step “1)”, “2)” and “3)”? Saying that they are independent, I would re-name them as Category A, B, C, ... or those names used in Figure 6.

Response:

The emission clumps are categorized in three types. The first one is the power plants (point-source clumps) which was directly taken from the power plants in ODIAC (which was based on CARMA dataset) (step “A”) in the revised manuscript, see the response to Q11). The second and third types of clumps are both area clumps and they are defined in step “B”) and steps “1)”-“4)” (see the response to Q11 and the revised manuscript). The clumps in the second type all have a core which was identified as “urban” by ESRI urban map. The clumps in the third type do not have a core from ESRI urban map, but have a core whose emissions are above threshold-1. Step “1)” defines the potential grid cells to be included in any clump, but does not define any clump. Step “2)” defines the cores correspond to an ESRI urban areas. Step “3)” defines other cores outside the ESRI urban area. Step “4)” attributes the grid cells defined in step “1)” and outside the area in steps “2)” and “3)” to either ESRI cores or non-ESRI cores.

We prefer to call them “point-source clump”, “ESRI clump” and “non-ESRI clump”, because they are more detailed than just “A”, “B” and “C”. Because the whole text discussed the differences and features of the three clumps, using these detailed names will help readers without any difficulty recalling what “A” and “B” and “C” refer to.

We add in line 216: “...recognizing different segments/objects in a picture or photograph. **The clumps with an ESRI core (step 2) are called “ESRI clumps”, while the clumps with a non-ESRI core (step 3) are called “non-ESRI clumps” hereafter.** This step is illustrated in Fig. 3e...

14) Line 204: What is the difference between “cities” and “towns”?

Response:

We find that the ESRI urban map is not complete to cover all the emission hotspots. For example, Fig. 4b in the manuscript show that ESRI urban map only identify Beijing, Tianjin, Langfang, etc. But we do see some areas with strong emissions outside these ESRI-urban area from Fig. 4e in the manuscript. Because these areas are usually smaller (in terms of surface area) than the ESRI-urban area, and is not connected to ESRI-urban area, we call them “smaller populated area”. Because countries differ in the levels of administrative divisions, to avoid the confusion raised by the referee, we changed the word “towns” into “small cities”.

15) Line 266: “The clump with largest emission is Shanghai” Is it total emission or emission density?

Response:

It is the total emission. We revise the sentence: “... The clump with largest **annual** emission **budget** is Shanghai, which emits 47 Mt C per year...”

16) Line 272-274: I cannot understand these sentences. Shorten for clarity.

Response:

We revise the sentence into: “... This is because the southeast coast of China is densely populated even **atwithin** rural **places-areas** (yellow-green **outside the urban area of ESRI urban map** in Fig. 4e), and because the emission rates per capita is also high in China **compared to the world average** (Janssens-Maenhout et al., 2017). As a result, our algorithm finds **more**

non-ESRI clumps and larger area for each clump in China than other regions.”

17) Line 280: There are other data sets for power plants in China better than the CARMA data set, e.g. the MEIC inventory, which has been noticed by the authors.

Response:

MEIC inventory is used for comparison in Sect. 3.2. In this part, we only discussed the distribution of clumps based on the ODIAC map, because it is a global map that were derived consistently among countries. In the paper, we aim at some consistency between regions that allow comparisons. On the other hand, the methodology that is described in the paper can be applied to MEIC (China) or VULCAN (USA) datasets, among others, for more regional applications.

18) Figure 5: I do not understand why most emission clumps look like circles or dots in the four zoomed region. Is it a visual illusion?

Response:

In this figure, we only plotted the location with small dots rather than the size and shape of the clumps. At continental scale, it is hard to display the precise shape of the clumps, which was shown by Fig. 4 in the manuscript. To make it clearer, we revise the title of this figure: “**Figure 5** The spatial distribution of **emission-weighted center of the** emission clumps all over the globe. The inserted plots zooms over 4 regions that contain most of the clumps.”

19) Section 4: there are too many materials dropped in this part, among which the relationship is not very clear. If these discussions are independent, they can be organized in different parts under different headlines.

Response:

Following the reviewer’s suggestion, we rewrite this section with three sub-sections: “**4.1 Impacts of the sounding precision on the identification of emission clumps**” (with first two paragraphs in the original manuscript), “**4.2 Impact of using ODIAC on the identification of emission clumps**” (a newly added paragraph and the third paragraph in the original manuscript), “**4.3 Implication for future inversion studies**” (the last paragraph in the original manuscript).

20) Line 466: “a set of large emission clumps” for a large area or a large emission?

Response:

We revise the sentence: “In this study, we have identified a set of ~~large~~-emission clumps with large emission rates (in the unit of $\text{g C m}^{-2} \text{hr}^{-1}$) from a high-resolution emission inventory. ...”

21) Line 467: “This identification method identify”-> “This method identifies”.

Response:

We revise the sentence as the reviewer suggested.

22) Line 476: “Given actual atmospheric transport,”-> “Given actual atmospheric transport

condition,”.

Response:

We revise the sentence as the reviewer suggested.

Response to comments on “A global map of emission clumps for future monitoring of fossil fuel CO₂ emissions from space” by Y. Wang et al.

We thank the referee for reviewing our manuscript. Please find attached a point-by point reply to each of the comments raised by the referee with legible text and figures organized along the text. Please find below the point-to-point responses (in black) to all referee comments (in blue). For your convenience, changes in the revised manuscript are highlighted with dark red. All the pages and line numbers correspond to the original version of text.

This paper presents an algorithm for generating distributions of CO₂ emission hotspots based on a high-resolution proxy. It applies this algorithm to generate such a distribution for 2016. It assesses the sensitivity of the distribution to parameters in the algorithm.

The paper is probably in scope for ESSD. My only concern is that it adds value to an existing data product rather than generating significant new data itself. Its main contribution is likely to be the clumping algorithm it uses and I urge the authors to make the algorithm as well as the data available. The paper is also clearly written and presented.

Response:

We would like to thank the referee for the valuable comments and suggestions for improving our manuscript.

Indeed, the algorithm presented in this paper is one of the major assets of this paper. The algorithm can be applied to other high-resolution emission maps (Sect. 3.2). Apart from the algorithm itself, Sect. 3.2 showed some consistencies between the results derived from ODIAC and those based on other emission maps. Given such consistencies algorithm, the complexity and the value of the algorithm, we think that this paper is in scope for ESSD: “Articles on methods describe nontrivial statistical and other methods employed (e.g. to filter, normalize, or convert raw data to primary published data) as well as nontrivial instrumentation or operational methods.” (https://www.earth-system-science-data.net/about/aims_and_scope.html).

We have published the dataset at <https://doi.org/10.6084/m9.figshare.7217726.v1>. And we provide the code in the supporting information.

I believe the paper makes a significant contribution. My main concern is some unexamined assumptions. Most crucially the underlying data set is not a true map of emissions but of emission proxies, mainly nighttime lights plus off-line estimates of emissions from power-stations. The spatial distribution of the proxy might well differ systematically from that of real emissions. In particular, there is a good chance that onroad emissions have greater spatial extent around emission cores than nighttime lights and may serve to amalgamate proximal clumps. This is testable now since the recent VULCAN product is available at the same resolution and includes these emissions. I recommend running the algorithm over VULCAN and ODIAC within the contiguous U.S. for the same year and comparing results.

Response:

We appreciate that the reviewer confirm the contribution of this study to the community.

The suggestion by the reviewer is indeed an important one. We are aware that we can't assume an emission field from a single emission dataset as perfect. As pointed out by the reviewer, ODIAC might miss some of the on-road emissions in the emission distribution due to the use of nighttime emission proxy. Following the reviewer's suggestion, we run the algorithm over the new version of the VULCAN emission data product (VULCANv3.0) provided by Prof. Gurney, one of the co-authors of this manuscript, and compare the results with the one based on ODIAC. The VULCANv3.0 use detailed primary data sets across the US. In the new version of VULCAN, they are in principal the same collection of datasets as described in Gurney et al. (2009), but with improvements in the data quality. The VULCANv3.0 also improves the spatial and temporal resolution compared to VULCANv2.2 (Gurney et al., 2009).

Fig. R1 shows the clump results based on ODIAC (a-f) and VULCANv3.0 (g-l) in the vicinity of three mega cities in US. The emission field in ODIAC are much smoother than that in VULCANv3.0. In VULCANv3.0, there are a large amount of small clumps around the large cities. Some of these small clumps correspond to the on-road emissions (e.g. long and narrow lines), and some correspond to small cities. For the on-road emissions, the algorithm sometimes split the road into several segments (e.g. the Pacific Coast Highway, Fig. R1h). In total, the ODIAC clumps covers 58% of the emissions in VULCANv3.0, while the emissions from on-road transportation and small cities that are missed by ODIAC clumps account for 27% of the total emissions in VULCANv3.0. This result is similar to that discussed in the manuscript Sect. 3.2, indicating some consistencies between the clump results derived from different emission products.

We would like to note that VULCANv3.0 is not yet publicly available, and that ESSD does not recommend to include such data (see Carlson and Oda, 2018 ESSD). Following the recommendation by the editor, we have not included this comparison in the manuscript. However, we discuss the limitation of the single use of the ODIAC product, which used nighttime light as a proxy for emissions in Sect. 4.2.

“4.2 Impact of using ODIAC on the identification of emission clumps

ODIAC used nighttime light as a proxy for the spatial distribution of emissions. The accuracy of the proxy in representing the distribution of actual emissions largely impacts the extent of the clumps. For example, compared with other emission products, ODIAC does not capture line source emissions such as on-road transportation (Oda et al., 2018; Gurney et al., 2019). The satellite observations of CO indicated significant CO enhancement over major roads (Borsdorff et al., 2019). Since our clump map is derived from ODIAC emission product, some of the roads that generate significant XCO₂ plumes may be missed by the clumps defined in this study. As the ODIAC team is planning to include transportation network data in their emission product (Oda et al., 2018), our clump map could be updated with a new version of ODIAC,

~~The emission clumps is a valuable concept relevant for the monitoring of fossil fuel CO₂-emissions from satellites.~~ Fig. 8 shows that... ”

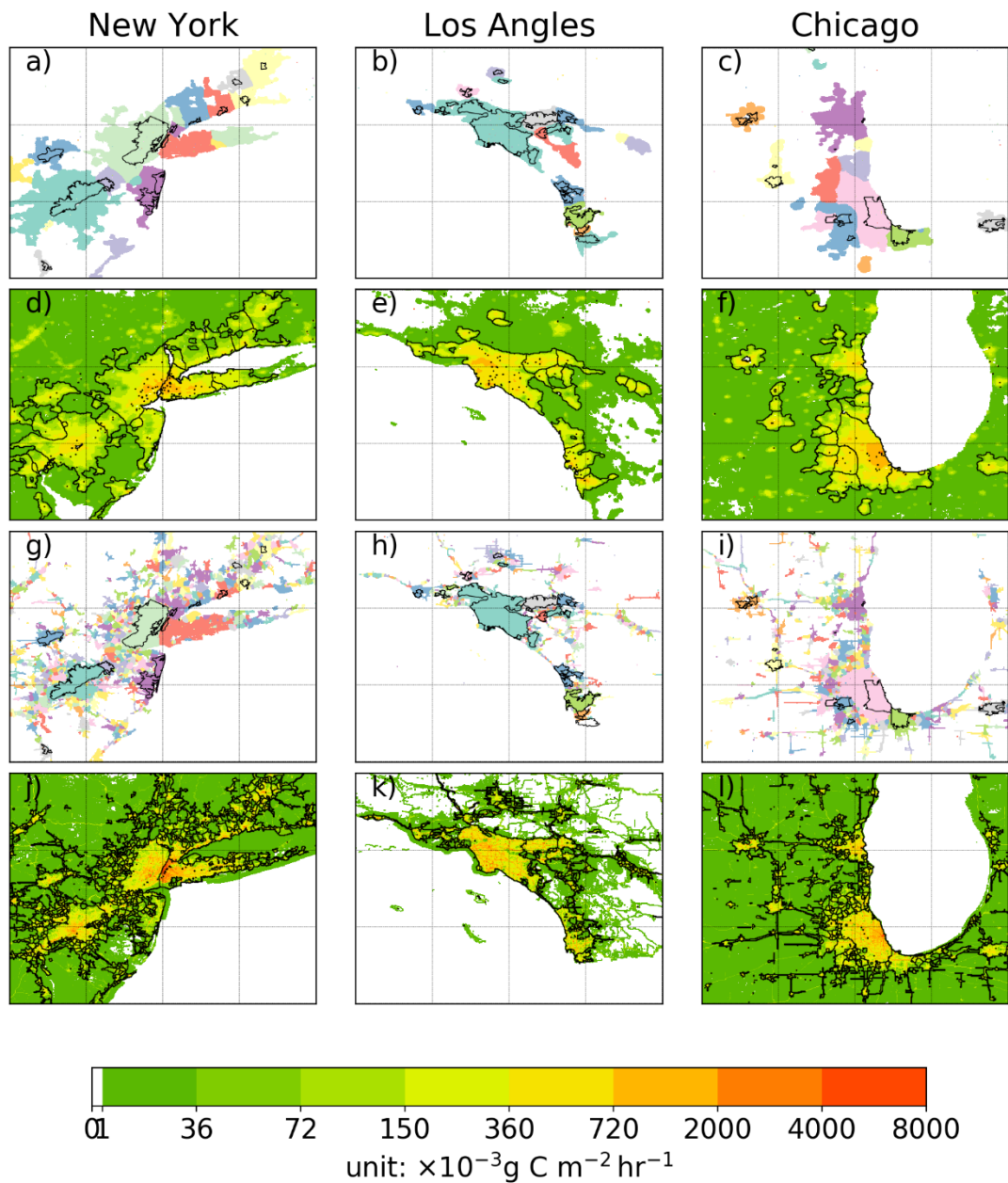


Figure R1 Emission clumps near New York (a, d, g and j), Los Angeles (b, e, h and k) and Chicago (c, f, i and l) based on ODIAC product (a-f) and VULCANv3.0 (g-l). In a-c and g-i, solid lines depict the urban areas from ESRI product. Colored patches depict the clump area. In d-f and j-l, solid lines depict the boundaries of final clumps (boundary of colored patches in a-c and g-i). Colored fields in d-f show the emissions from ODIAC product. Colored fields in j-l show the emissions from VULCANv3.0. Light dashed lines indicate $1^\circ \times 1^\circ$ grids.

Some specific comments

1) L140 I did not think the DMSP lights were available for 2016 but that ODIAC had switched to VIIRS.

Response:

The ODIAC model employs the DMSP radiance calibrated nighttime light products (https://www.ngdc.noaa.gov/eog/dmsp/download_radcal.html) for estimating emission spatial distributions of non-point emissions (see Oda et al. 2018). As the reviewer pointed out, the DMPS data are not available for the year 2016 (the latest radiance calibrated data is for year 2010). The current ODIAC model uses the 2010 DMSP nighttime light product for the period 2010-2017. As mentioned in Oda et al. (2018), the research team plans to use the VIIRS nightlight for future versions of the ODIAC emission product development. But the version of the ODIAC data product used in this study (ODIAC2017) is still based on the DMSP nighttime light data.

2) L240 Probably there is no need to mention the python version though pointing out the package used is good. Note my firm suggestion above that the algorithm be made available.

Response:

To maintain the traceability and reproducibility, we provide all the computer codes that is used to produce the emission clumps presented in this study, with detailed comments.

References:

- Carlson, D. and Oda, T.: Editorial: Data publication – ESSD goals, practices and recommendations, *Earth System Science Data*, 10(4), 2275–2278, doi:<https://doi.org/10.5194/essd-10-2275-2018>, 2018.
- Gurney, K. R., Mendoza, D. L., Zhou, Y., Fischer, M. L., Miller, C. C., Geethakumar, S. and Can, S. de la R. du: High Resolution Fossil Fuel Combustion CO₂ Emission Fluxes for the United States, *Environmental Science & Technology*, 43(14), 5535–5541, 2009.

5 **A global map of emission clumps for future monitoring of fossil fuel CO₂ emissions from space**

Yilong Wang^{1,*}, Philippe Ciais¹, Grégoire Broquet¹, François-Marie Bréon¹, Tomohiro Oda^{2,3}, Franck Lespinas¹, Yasjka Meijer⁴, Armin Loescher⁴, Greet Janssens-Maenhout⁵, Bo Zheng¹, Haoran Xu⁶, Shu Tao⁶, [Kevin R. Gurney⁷](#), [Geoffrey Roest⁷](#), Diego Santaren¹, Yongxian Su^{7,8}

10 ¹Laboratoire des Sciences du Climat et de l'Environnement, CEA-CNRS-UVSQ- Université Paris Saclay, 91191, Gif-sur-Yvette CEDEX, France

²Global Modeling and Assimilation Office, NASA Goddard Space Flight Center, Greenbelt, MD, USA

³Goddard Earth Sciences Technology and Research, Universities Space Research Association, Columbia, MD, USA

⁴European Space Agency (ESA), Noordwijk, Netherlands

15 ⁵European Commission, Joint Research Centre, Directorate Sustainable Resources, via E. Fermi 2749 (T.P. 123), I- 21027 Ispra, Italy

⁶Laboratory for Earth Surface Processes, College of Urban and Environmental Sciences, Peking University, Beijing, China

⁷[School of Informatics, Computing and Cyber Systems, Northern Arizona University, Flagstaff, AZ 86011, USA](#)

20 ⁸⁷Key Lab of Guangdong for Utilization of Remote Sensing and Geographical Information System, Guangdong Open Laboratory of Geospatial Information Technology and Application, Guangzhou Institute of Geography, Guangzhou 510070, China

*Correspondence to: Yilong Wang (yilong.wang@lscce.ipsl.fr)

Abstract. A large fraction of fossil fuel CO₂ emissions ~~occur within~~ emanate from “hotspots”, such as cities (where direct CO₂ emissions related to fossil fuel combustion in transport, residential, commercial sectors, etc., excluding emissions from electricity-producing power plants, occur), isolated power plants, and manufacturing facilities ~~and power plants~~, which cover a very-small fraction of the land surface. ~~Although some of these emission hotspots are monitored closely, there is no detailed emission inventory for most of them.~~ The coverage of all high-emitting cities and point sources across the globe by bottom-up inventories is far from complete, and for most of those covered, the uncertainties in CO₂ emission estimates in bottom-up inventories are too large to allow continuous and rigorous assessment of emission changes (Gurney et al., 2019). Space-borne imagery of atmospheric CO₂ has the potential to provide independent estimates of CO₂ emissions from hotspots. But first, what is a hotspot needs to be defined for the purpose of satellite observations. The proposed space-borne imagers with global coverage planned for the coming decade have a pixel size on the order of a few square kilometers, and a XCO₂ accuracy and precision of <1 ppm for individual ~~pixels~~ measurements of vertically integrated columns of dry air mole fractions of CO₂ (XCO₂). This resolution and precision is insufficient to provide a cartography of emissions for each individual pixel. Rather, the integrated emission of ~~the~~ diffuse emitting areas and ~~the~~ intense point sources are sought. In this study, we ~~address the question of the global characterization of~~ characterize area and point fossil fuel CO₂ emitting sources (~~those hotspots are called emission clumps hereafter~~) that may cause generating coherent XCO₂ plumes that may be observed from in ~~space-borne CO₂ images.~~ We characterize these emitting sources around the globe and they are referred to as “emission clumps” hereafter. An algorithm is proposed to identify emission clumps worldwide, based on the ODIAC global high resolution 1 km fossil fuel

25
30
35
40

emission data product. The clump algorithm selects the major urban areas from a GIS (geographic information system) file and two emission thresholds. The selected urban areas and a high emission threshold are used to identify clump cores such as inner city areas or large power plants. A low threshold and a random walker (RW) scheme are then used to aggregate all grid cells contiguous to cores in order to define a single clump. With our definition of the thresholds, which are appropriate for a space imagery with 0.5 ppm precision for a single XCO₂ measurement, a total of 11,314 individual clumps, with 5,088 area clumps and 6,226 point-source clumps (power plants), are identified. These clumps contribute 72% of the global fossil fuel CO₂ emissions according to the ODIACS inventory. The emission clumps is a new tool for comparing fossil fuel CO₂ emissions from different inventories, and objectively identifying emitting areas that have a potential to be detected by future global satellite imagery of XCO₂. The emission clump data product is distributed from <https://doi.org/10.6084/m9.figshare.7217726.v1>.

1 Introduction

Monitoring the effectiveness of emission reductions after the Paris Agreement on Climate (UNFCCC, 2015) requires frequently updated estimates of fossil fuel CO₂ emissions and a global synthesis of these estimates. The need for emission monitoring goes beyond national estimates, as many cities and regions have set concrete objectives to reduce their greenhouse gas emissions. The CO₂ emissions (direct and indirect) related to final energy use in cities are estimated to be 71% of the global total (IEA, 2008; Seto et al., 2014). In addition, power plants account for ~40% of direct energy-related CO₂ emissions (~~Tong et al., 2018~~), and are subject to regulations that require a regular reporting of their emissions. The contribution from cities (excluding electricity-related emissions from large power plants, see Sect. 2) and power plants to national and global mitigation efforts is thus critical (Creutzig et al., 2015; Shan et al., 2018).

~~Research to quantify emissions based on prior information on their magnitude and distribution, atmospheric CO₂ concentration measurements and atmospheric transport models is a branch of science called atmospheric CO₂ inversions. The technique called atmospheric CO₂ inversion quantifies emissions based on a prior estimate from inventories, atmospheric CO₂ measurements and atmospheric transport models.~~ Inversions of fossil fuel CO₂ emissions have used in-situ surface networks, aircraft measurements and mobile platforms around cities (Brón et al., 2015; Lauvaux et al., 2016; Staufer et al., 2016), but the deployment of a network around each city may be impractical. Alternatively, it is possible to measure vertically integrated columns of dry air mole fractions of CO₂ (XCO₂) from satellites passing over emission hotspots. Satellite measurements offer the advantage of global spatial coverage, but research studies consistently outlined that satellite XCO₂ measurements need to have a high precision (< 1 ppm) and a spatial sampling at high resolution (< 2-3 km horizontal resolution) (Bovensmann et al., 2010; O'Brien et al., 2016). For example, the Greenhouse Gases Observing Satellite (GOSat-2) aims to measure XCO₂ at 0.5 ppm precision (<https://directory.eoportal.org/web/eoportal/satellite-missions/g/gosat-2>). The single sounding random error in XCO₂ from the Orbiting Carbon Observatory 2 (OCO-2) is on the order of magnitude of 0.5 ppm (Eldering et al., 2017;

Chatterjee et al., 2017). XCO₂ measurements from selected 10 km wide OCO-2 tracks downwind of large power plants were used to quantify their emissions by fitting observed XCO₂ plumes with Gaussian dispersion models (Nassar et al., 2017). According to Nassar et al., (2017), the uncertainties in the emissions from three selected U.S. power plants were constrained within 1–17% of reported daily emission values. The primary scientific goal of the OCO-2 mission was to estimate natural land and ocean carbon fluxes, and tracks overpassing power plants are very sporadic, given the narrow swath width and frequent clouds. In order to improve the sampling of the atmosphere, XCO₂ imagers (e.g. passive spectral-imagers in the short wave infrared spectrum) are under study. The list includes the Geostationary Carbon Observatory (GeoCARB) mission (Polonsky et al., 2014), the OCO-3 instrument on board the International Space Station capable of pointing to chosen emitting areas (https://www.nasa.gov/mission_pages/station/research/experiments/2047.html) and a constellation of low earth orbiting (LEO) imagers with a swath of a few hundred kilometers planned as future operational missions within the European Copernicus Program (Ciais et al., 2015).

The ability of imaging instruments to reduce uncertainty on CO₂ emissions was investigated by atmospheric inversions with pseudo-data, that is, Observing System Simulation Experiments (OSSEs), but only for case studies of limited duration. OSSEs were performed for large cities (Broquet et al., 2018; Pillai et al., 2016), single power plants (Bovensmann et al., 2010) or for a region encompassing several cities (O’Brien et al., 2016). An OSSE study with one LEO imager over Paris (Broquet et al., 2018) solved for emissions during the 6 h before a given satellite overpass. Their results showed that the uncertainty (~25%) in the 6 h mean emissions in the prior estimates could be reduced to less than 10% during few days when the wind speed is low and there is not much cloud. The results of such case studies are informative about the potential of satellite observations in quantifying fossil fuel CO₂ emissions, but do not inform systematically about how many hotspots, and which fraction of emissions worldwide could be constrained with XCO₂ imagers.

A prerequisite for assessing the capability of satellite imagers is to have a high resolution global map of fossil fuel CO₂ emissions (Gurney et al., 2019). We use in this study the ODIAC map at 30×30 arc-seconds (~ 1 km×1 km) (Sect. 2.1). Not all the emitting 1 x 1 km land grid-cells of such a map will have emissions sufficiently intense to produce a XCO₂ plume detected with a satellite (Nassar et al., 2017; Hakkarainen et al., 2016). On the other hand, a cluster of contiguous emitting grid cells will create a stronger plume than a single emitting grid cell, so that the uncertainty on the sum of emissions from a cluster could be reduced with space-borne measurements. This poses the research question of how to define those clusters of emitting pixels (called emission clumps hereafter) who will generate individual XCO₂ plumes being detectable from space. The emission clumps should include intense area sources and large isolated point sources (e.g. power plants, large factories). Using political and administrative area of cities to define clumps does not work for this purpose because the same administrative area may contain separate large point sources or multiple hotspots forming separable plumes, as well as areas with no or little emission. The definitions of emitting areas differ among inversion studies. Broquet et al. (2018) estimated emissions from the Île de France region, while Pillai et al. (2016) defined their emitting region as an area of 100 km×100 km around Berlin. The arbitrary choice of emitting areas across studies make the comparison of their results difficult and are not applicable worldwide.

105 This justifies the need for a systematic and objective definition of emission clumps that constitute observing targets for satellites.

The algorithm for calculating emission clumps developed in this study is inspired by research on mapping urban area and socio-demographic activities (Li and Zhou, 2017; Elvidge et al., 1997; Zhou et al., 2015; Su et al., 2015; Doll and Pachauri et al., 2010; Letu et al., 2010). The corresponding algorithms can be grouped in classification-based or threshold-based. Classification-based algorithms use datasets such as the normalized difference vegetation index (NDVI) and the normalized difference water index (NDWI) to train a machine-learning model to classify urban and non-urban areas (Cao et al., 2009; Huang et al., 2016). Threshold-based algorithms classify urban grid cells where some continuous variables (e.g. nighttime lights) are above a given threshold (Elvidge et al., 1997; Liu and Leung, 2015; Li et al., 2015; Liu et al., 2015). In threshold-based methods, given the high spatial heterogeneity of urbanization and urban forms, efforts have been devoted to finding local optimal thresholds, such as the “light-picking” approach to find a local nighttime background light surrounding a target grid cell (Elvidge et al., 1997), or determining local thresholds by matching local/site-based surveys and land-use/land-cover (LULC) datasets (Zhou et al., 2014).

The problem of characterizing CO₂ emission clumps posed here consists in delineating all areas that have a potential to generate detectable atmospheric XCO₂ plumes. “Detectable” means here that the concentration within a plume formed by a clump should be large enough compared to the surrounding background in XCO₂ images of typical spatial resolution of ≈1 km. The magnitude of a minimum detectable XCO₂ enhancement in a plume (relative to the surrounding background) depends on the individual XCO₂ sounding precision. Such sounding precision should be of a similar order of magnitude worldwide, although the solar zenith angle, aerosol loads, surface albedo etc. will affect it (Buchwitz, et al., 2013). In this context, contrary to the algorithms used for mapping urban areas, common global minimum emission thresholds for land grid cells forming a clump are relevant.

Because CO₂ produced by emissions is quickly dispersed by transport, XCO₂ plumes sampled at a given time by a satellite image usually relate to emissions that occurred few hours before its acquisition (Broquet et al., 2018). In this study, we focus on planned LEO imagers on Sentinel missions, assuming an equator crossing time around 11:30 local time (Buchwitz et al., 2013; Broquet et al., 2018) so that XCO₂ plumes sampled by these imagers are from morning emissions. Different overpass times are also possible for other satellites. For example, Equator crossing times of OCO-2 and GOSAT are 13:00-13:30 local time. Geostationary imagers may provide a better temporal coverage of the emissions; e.g. GeoCARB images are considered to sample a city for multiple times within a day (O’Brien et al., 2016).

This study aims to provide a global dataset of fossil fuel CO₂ emission clumps for high-resolution atmospheric inversions that will use XCO₂ imager data. Such a dataset can be used for OSSE studies to compare different imagery observation concepts for constraining fossil fuel CO₂ emissions at the clump scale over the whole globe. We propose an approach that combines a threshold-based and an image-processing algorithm. Section 2 describes the high-spatial resolution global emission map upon which clumps are calculated, and the algorithm to delineate the clumps worldwide. The spatial distribution and extent of the

140 resulting clumps throughout the globe are described in Sect. 3 and are compared with clumps diagnosed by applying the same algorithm to other emission maps. Section 4 discusses the sensitivity of the resulting clumps to the precision of XCO₂ measurements and future applications of this global dataset. Section 5 describes the data availability. Conclusions are drawn in Sect. 6.

2. Methodology

2.1 ~~ODIAC fossil fuel CO₂ emission map~~ Development of a high resolution emission map of morning emissions

145 We use the high-spatial resolution (30" × 30" ≈ 1 km × 1 km) global annual fossil fuel CO₂ emission map for the year 2016 from the Open Source Data Inventory of Anthropogenic CO₂ Emission (ODIAC, version 2017) (Oda and Maksyutov, 2011; Oda et al., 2018) for calculating clumps. To our knowledge, it is the only emission map with global coverage and a spatial resolution high enough to match the pixel size of ≈ 1 km of atmospheric XCO₂ imagers. We chose the year 2016 assuming that the emission spatial distributions do not change significantly from year to year. In regions with rapid urbanization rates, the emission spatial distributions may change rapidly. The analysis of such changes is out of the scope of this paper, but the clump definition can be updated consistently with the latest high-resolution emission maps for each year, using the approach presented in Sect. 2.2. The ODIAC dataset provides emissions from power plants based on the CARMA database (Carbon Monitoring and Action, <http://carma.org>). Emissions from these point sources were spatially allocated to the exact locations from CARMA. Emissions from other sources (industrial, residential, commercial sectors and daily land transportation) were estimated by subtracting the sum of emissions from power plants in each country from the national totals given by the Carbon Dioxide Information and Analysis Center (CDIAC) (Boden et al., 2016). Annual emissions in each country excluding power plants were spatially distributed at 30" spatial resolution using nighttime light fields from the Defense Meteorological Satellite Program (DMSP) satellites. ODIAC has been used in atmospheric inversions to monitor CO₂ emissions from cities (Oda et al., 2018; Lauvaux et al., 2016).

160 ~~Because CO₂ produced by emissions is quickly dispersed by transport, XCO₂ plumes sampled at a given time by a satellite image usually relate to emissions that occurred few hours before its acquisition (Broquet et al., 2018). Here we assumed an equator crossing time around 11:30 local time for LEO imagers on Sentinel missions (Buchwitz et al., 2013; Broquet et al., 2018), so that XCO₂ plumes sampled by these imagers are from morning emissions. Different overpass times are also possible for other satellites. For example, Equator crossing times of OCO 2 and GOSAT are 13:00-13:30 local time. Geostationary imagers may provide a better temporal coverage of the emissions; e.g. GeoCARB images are considered to sample a city for multiple times within a day (O'Brien et al., 2016).~~

165 ~~We adopt here a focus on planned Sentinel LEO imagers, and thus use annual average of morning emissions for calculating emission clumps.~~ To estimate morning emissions, we combined the ODIAC emission maps with the hourly profiles from the Temporal Improvements for Modeling Emissions by Scaling (TIMES) product (Nassar et al., 2013). In TIMES, the

hourly profiles were provided as 24 scaling factors for each hour of the day that can be multiplied by daily average emissions to derive hourly emissions. Hourly scaling factors of TIMES were derived for residential, commercial, industrial, electricity production and mobile on-road sectors from the bottom-up model of fossil fuel CO₂ emissions Vulcan v2.0 over the US (Gurney et al., 2009) with mobile non-road, cement manufacture and aircraft assumed temporally constant. The TIMES dataset also gives hourly scaling factors for ~~other-19~~ other high-emitting countries. These profiles were weighted by the emissions fraction in each sector from EDGAR to determine hourly profiles of total CO₂ emissions. The US and ~~other-19~~ other high-emitting countries are called “proxy” countries. Other countries in the world were assigned ~~the same profiles than~~ one of the proxy country profiles, accounting for standard international time zones, and local socio-demographic patterns (e.g. time of day when people start to work, weekend defined according to different religions). The TIMES hourly profiles were derived at the national scale (assuming identical hourly profiles within a country) and then shifted by hourly offsets according to local solar time to approximate the variability related to geophysical cycles. The original TIMES hourly profiles at 0.25 °×0.25 ° resolution were downscaled to at the spatial resolution of ODIAC, assuming the same profiles within each 0.25 °×0.25 ° grid cell. For calculating clumps based on morning emissions, we multiplied the annual mean emission rate (unit: g C m⁻² hr⁻¹) in each grid cell of ODIAC by the average scaling factors of emissions between 6:00-12:00 local time. The day-to-day and month-to-month variations in the spatial distribution of fossil fuel CO₂ emissions may lead to temporal variations in the spatial extent of the clumps. In this study, we define the clumps based on two thresholds (see Sect. 2.2) to ensure that the effective clumps are always within the boundaries of the clumps, and that the satellite observation should provide emission estimates consistently within a year. We thus ignore the month-to-month and day-to-day variations in the emissions.

2.2 Calculation of emission clumps

The emission clumps from point sources and intense area sources in ODIAC are separated in this study. In ODIAC, the point sources only refer to power plants in the CARMA database. So in this study, we refer to sources other than power plants as area sources. Before clumps are calculated, Fig. 1 illustrates the ranked distribution of emission rates during morning hours from point sources (red) and other grid cells (blue). Excluding emissions from point sources, the maximum emission rate of emitting grid cells from area sources is 20.7 g C m⁻² hr⁻¹ and most grid cells including point sources have much larger emission rates than this value. In total, 35% of the global total emissions are from 12433 30" ×30" grid cells encompassing at least one point source.

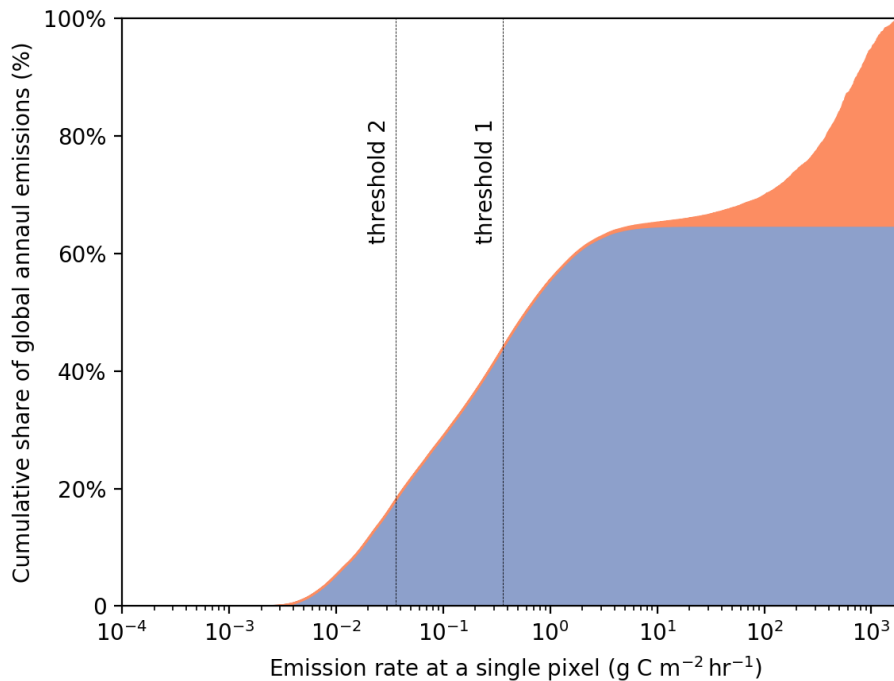


Figure 1 Cumulative distribution of mean emission rates during morning hours in ODIAC for power plants (red) and area sources (blue). The y-axis represents the cumulative share of global total annual emissions at each level of emission rate for a single land grid cell (x-axis). The vertical dash lines are the two thresholds used in the clump algorithm (see text).

Figure 2 shows the flowchart of the clump algorithm. Fig. 3 illustrates how it operates for a small domain as an example.

Two categories of emission clumps are defined:

A) Firstly, o Only grid cells encompassing point sources with an emission rate larger than threshold-1 are considered. This threshold is chosen as $0.36 \text{ g C m}^{-2} \text{ hr}^{-1}$, based on the argument that, even without any atmospheric horizontal transport, emissions lower than this threshold over 6 hours would generate a local XCO_2 excess of less than 0.5 ppm, the practical limit of individual sounding precision from current satellites (see Appendix for the detailed computation). This is illustrated in Fig. 3b by the red grid cell labeled as 1 and 2. There are 6226 grid cells in ODIAC2017 who encompass at least one power plant and whose emission rates are above threshold-1, which account for >99.99% of total emissions of all CARMA power plants globally.

Secondly, B) e Emissions clumps from area sources are calculated. We combine two data streams to calculate area clumps: 1) the administrative division of major urban areas; and 2) two thresholds (threshold-1 and threshold-2 detailed below) applied to the grid cells of ODIAC. We assume that a group of emitting pixels encompassing some adjacent high emitting pixels (forming a core of the emission clump) and their surroundings will generate an individual plume in XCO_2 . The urban area and the high threshold (threshold-1) define the cores of each emission clump, while threshold-2 defines the lower limit of surrounding emitting pixels to be potentially included in the clumps. The four steps to compute area sources emission clumps

are detailed as below.

1) The value of threshold-2, above which emissions of a single emitting grid cell is selected to be potentially included in a clump, is chosen as $0.036 \text{ g C m}^{-2} \text{ hr}^{-1}$, a factor of 10 lower than threshold-1. The sum of emissions from grid cells above threshold-2 represents 82% of global total emissions (including point sources). Grid cells below threshold-2 are never included in any emission clump. Grid cells whose emission rates are above threshold-2 are illustrated in Fig. 3a by the yellow and orange grid cells;

2) We then used the urban area GIS (geographic information system) file from the Environmental Systems Research Institute (ESRI, <https://www.arcgis.com/home/item.html?id=2853306e11b2467ba0458bf667e1c584>) to locate the geographic positions of major urban areas. ESRI contains 3615 separated urban areas, defined independently from the ODIAC emission map. We found 2017 ESRI urban areas containing at least one grid cell with emission above threshold-1. The remaining 1598 ESRI urban areas are not considered hereafter. An illustration of one of the 2017 selected ESRI urban area is shown in Fig. 3c by the grid cells labeled as 3. Figure 4a-4c (solid lines) shows three examples of ESRI urban areas for major cities in Europe, North America and China. The grid cells within the ESRI urban area whose emission rates are above threshold-1 define the cores of the clumps.

3) Although the ESRI GIS file cover large cities of the world, smaller populated areas, like small citiestowns on the southeast coast of China that may also generate detectable plumes, are missed by ESRI map. This calls for a complementary step to identify non-ESRI emitting clumps. For the calculation of those non-ESRI clumps, we apply threshold-1 of $0.36 \text{ g C m}^{-2} \text{ hr}^{-1}$ to all grid cells that are not selected in the previous step as part of any ESRI core. Contiguous non-ESRI grid cells above threshold-1 form non-ESRI core of clumps. These non-ESRI core grid cells must be spatially distinct from the ESRI core grid cells. If they are adjacent to any ESRI core, they are absorbed by the ESRI ones. A total of 3071 non-ESRI cores are calculated, as shown in Fig. 3d by the grid cells labeled as 4;

4) After ESRI and non-ESRI clump cores are defined, we aggregate all the emitting grid cells whose emission rates are larger than threshold-2 in their vicinity to form a clump. An ensemble of grid cells with emissions higher than threshold-2 in a domain with N cores are attributed to N distinct emission clumps. The attribution of a grid cell to a given core is calculated based on the spatial gradients of emissions and the distance between the emitting grid cells by using a “random walker” (RW) algorithm (Grady, 2006). RW is a type of algorithm used in the field of image segmentation, i.e. recognizing different segments/objects in a picture or photograph. The clumps with an ESRI core (step 2) are called “ESRI clumps”, while the clumps with a non-ESRI core (step 3) are called “non-ESRI clumps” hereafter. This step is illustrated in Fig. 3e by the grid cells in light yellow.

The RW algorithm defines the probability of each grid cell to belong to some known labeled “seeds” (i.e. the cores defined in steps 2 and 3 in this study). This algorithm imagines that a random walker start from each grid cell to be labeled (in this study, the grid cells whose emissions that are above threshold-2 but not included in the cores). The probability that the walker will arrive at each known seeds, following the easiest path, are computed. The undefined grid cells are assigned to the seed

that has the highest probability to be reached by the walker. Specifically, in this study, we define the probability that the walker
250 move between two neighboring grid cells using an exponential decaying function of the ℓ^2 norm of the log-transformed local
gradients in emissions (Grady, 2006):

$$w_{ij} = e^{-\beta(g_i - g_j)^2} \quad (1)$$

where w_{ij} is the probability of motion between neighboring grid cells i and j , g_i and g_j are image intensity (defined as the log-
transformed emission rate in this study), and β is a free penalization parameter for the motion of random walker (the greater
255 the β , the more difficult the motion). In this study, β only impacts how the undefined grid cells are assigned to the cores. It
balances the effect of local gradients and the distance of the path from the undefined grid cells to the seeds: the larger the
gradients along a path between the undefined grid cells and the seeds, the smaller probability that the walker would move; and
the longer the path, the smaller the probability that the walker would arrive at corresponding seeds. Larger β will lead to larger
impact of emission gradients than that of distance. In this study, $\beta=13 \sigma_g^{-1}$, where σ_g is the standard deviation of the emission
260 rates at all the grid cells in ODIAC. In general, the algorithm can effectively separate different clusters of grid cells with
different spatial distributions. For instance, a clump with a flat distribution of emissions and a clump (of similar size as the
former one) with more skewed emissions are separated near the steepest gradients. This assumes that large emission gradients
will generate large gradients in XCO_2 (given similar meteorological condition for neighboring clumps), and that different
 XCO_2 plumes are separable where the XCO_2 gradients are the largest.

265 After the RW algorithm, grid cells above threshold-2 that are not contiguous to any core are discarded. This removes 10%
of the total from the 82% of global emissions defined in step 1. As a result, 72% of the global emissions are included in the
emission clumps (see more detailed discussion below).

All the computation are made under the Python version 2.7 environment (Python Software Foundation,
270 <http://www.python.org>) and the RW algorithm is from package “scikit-image” version 0.14dev (<http://scikit-image.org/>).

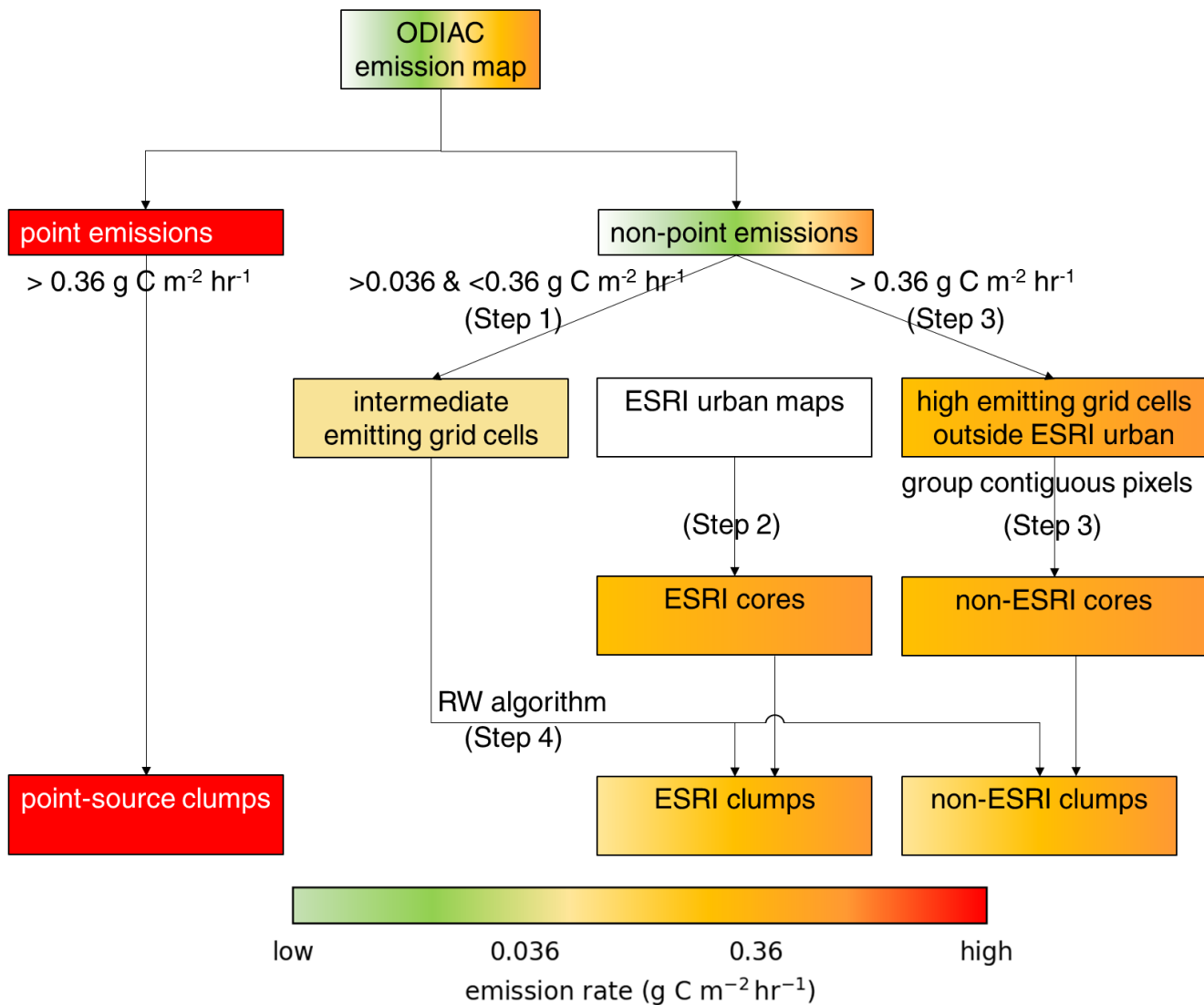


Figure 2 The flow chart of emission clumps calculation. The colors qualitatively illustrate grid cell emission rates from low (light green) to high (red)

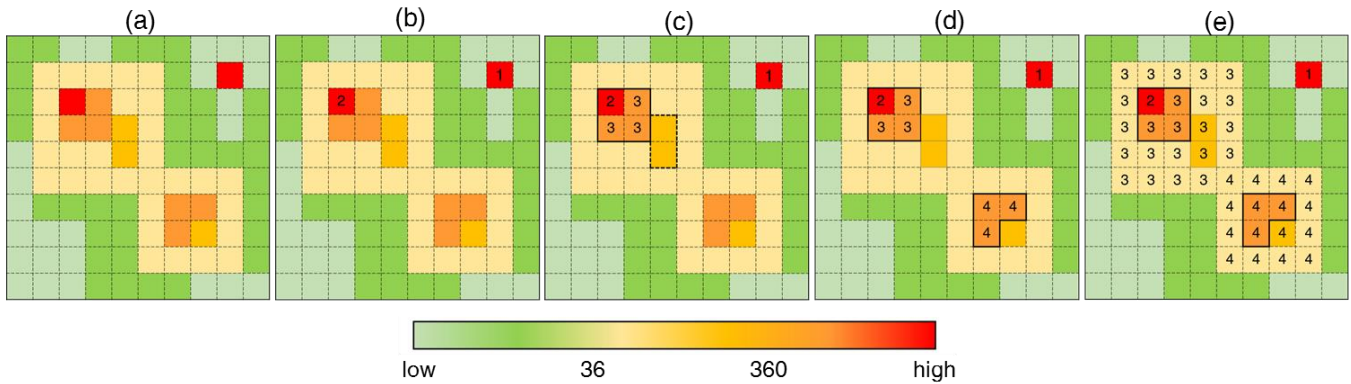


Figure 3 The processes of defining emission clumps. The colors qualitatively illustrate the emission rates from low (light green) to high (red). a) the emission field; b) 2 power plant (red grid cells) is defined as two individual clumps, labelled as 1 and 2; c) The ESRI urban area is outlined by bold solid and dashed lines, but the ESRI core is labelled as 3 only for grid cells whose emission rates are above threshold-1; d) the orange area represent grid cells whose emissions are above threshold-1 to form a non-ESRI core, labelled as 4; e) each light-yellow grid cell is assigned to one of the clump cores using the RW algorithm (see the main text). Note that one power plant (labelled 2) is located within the ESRI urban area, but is identified as a different emission clump from the ESRI clump (labeled as 3 in Fig. 3e)

3. Results

3.1 Emission clumps defined on ODIAC emission map

Figure 4 shows three regional clumps near Paris (France), New York (USA) and Beijing (China). The clumps near Paris are well isolated from each other. There are more emission clumps in the New York region. Because some clumps are close to each other in this region (e.g. New York and Clifton), their plumes will only be distinct when the wind direction is roughly perpendicular to the direction of the line connecting clumps (i.e. from southwest to northeast or the opposite for New York and Clifton). Near Beijing, there are a larger number of clumps than in the other two regions and their distribution is also more complex.

Table 1 summarizes the clumps calculated for the globe, Europe (European Russia included), China, North America, South America, Africa, Australia and Asia (China excluded). In total, our algorithm calculates 11314 clumps, including 6226 point sources, 2017 ESRI clumps, and 3071 non-ESRI clumps. The clump with largest annual emission budget is Shanghai, which emits 47 Mt C per year. A large fraction of the non-ESRI clumps is found within China mainly located near the southeastern coast, which may be explained by the recent rapid urbanization (Shan et al., 2018; Wang et al., 2016) in this region. This is not documented by the ESRI map. The large number of non-ESRI clumps in China highlights the necessity to consider emitters outside the major cities (at least) in this country. In addition, the mean area of an emission clump is larger in China than over other continents/regions. This is because the southeast coast of China is densely populated even atwithin rural

300 ~~areas~~ (yellow-green outside the urban area of ESRI urban map in Fig. 4e), and because the emission rates per capita is also high in China compared to the world average (Janssens-Maenhout et al., 2017). As a result, our algorithm finds: ~~1) more cores (of non-ESRI clumps) in China than other regions; and 2) larger area with emission rates larger than threshold 2. more non-ESRI clumps and larger area for each clump in China than other regions.~~

305 Figure 5 shows the locations and annual emissions of the clumps. The densities of emission clumps are high in Europe, the East Coast of US, the East Coast of China and India. Fig. 6 shows the fractions of total emissions allocated to different clump categories. Globally, 27% of the clumps are calculated as non-ESRI, but the total emission from these clumps is less than 13% of the total emissions. Point sources form 55% of the total number of clumps and 44% of the total emissions. In China, however, point sources contribute only 21% of the total number of clumps and 39% of the total emissions, which may be explained by the fact that the power plants in China considered in CARMA dataset (and thus in ODIAC) are limited to the
310 few larger power plants. Fig. 7 shows the cumulative distribution of the number of clumps and their emission for a few regions. Among ESRI clumps, 66% of them have an annual emission below 1 Tg C yr⁻¹, but the cumulative emission from these low emitting clumps only account for 22% of the total emissions from all ESRI clumps. The inflexion point in Fig. 7 (when the cumulative distribution curve turns from nearly 0% to a fast increase) indicates the importance of clumps whose annual emissions are above this value. For non-ESRI clumps and point sources, the inflexion points are near 0.1 Tg C yr⁻¹.

315

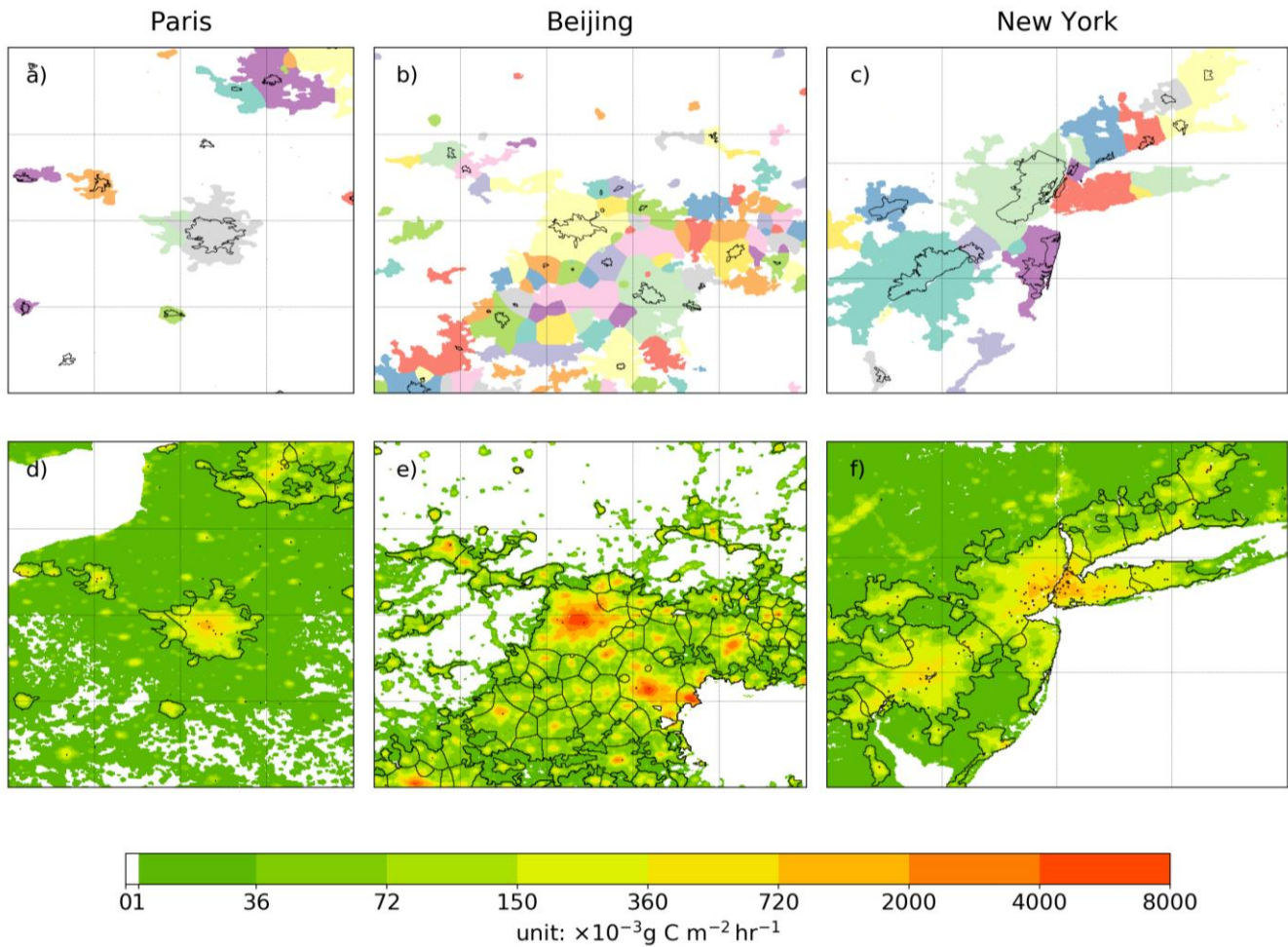
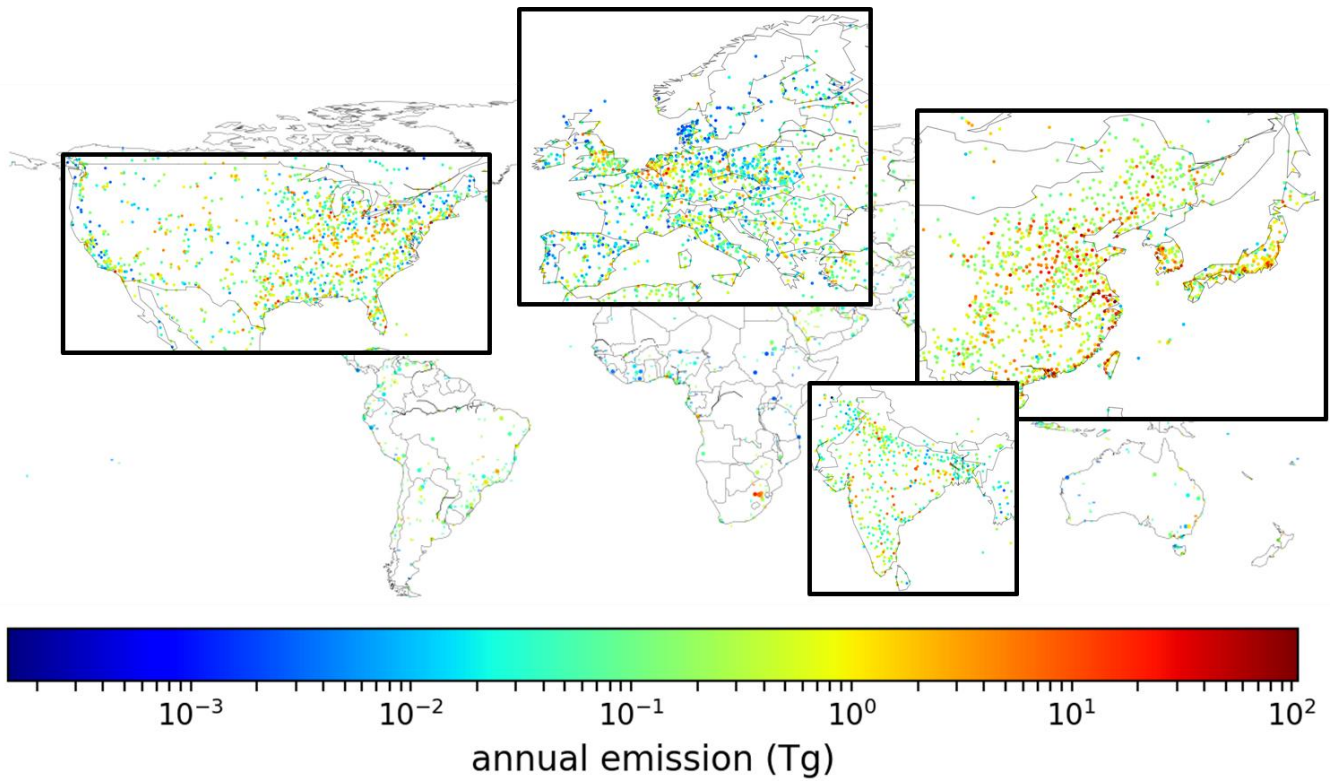
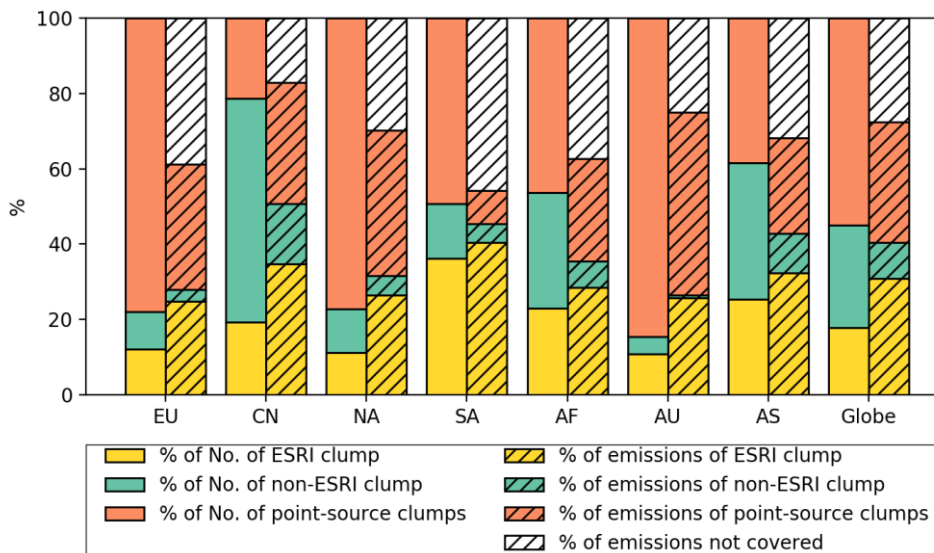


Figure 4 Emission clumps near Paris (a and d), Beijing (b and e) and New York (c and f). In a-c, solid lines depict the urban areas from ESRI product. Colored patches depict the clump area resulting from the algorithm defined in this study. In d-f, solid lines depict the boundaries of final clumps (boundary of colored patches in a-c). Colored fields in d-f show the emissions from ODIAC product. Light dashed lines indicate 1°x1° grids.

320



325 | **Figure 5** The spatial distribution of emission-weighted center of the emission clumps all over the globe. The inserted plots zooms over 4 regions that contain most of the clumps.



330 **Figure 6** The fraction of the number (bars) and the fraction of emissions (hatched bars) found in the three types of clumps for European continent (European Russia included), China, North America (NA), South America (SA), Africa, Australia, Asia with China excluded (AS) and over the globe. The three colors represent ESRI clumps (yellow), non-ESRI clumps (green) and point-source clumps (red), respectively. The white-hatched bars indicate the fraction of ODIAC emissions that are not allocated into any clump by the algorithm.

335

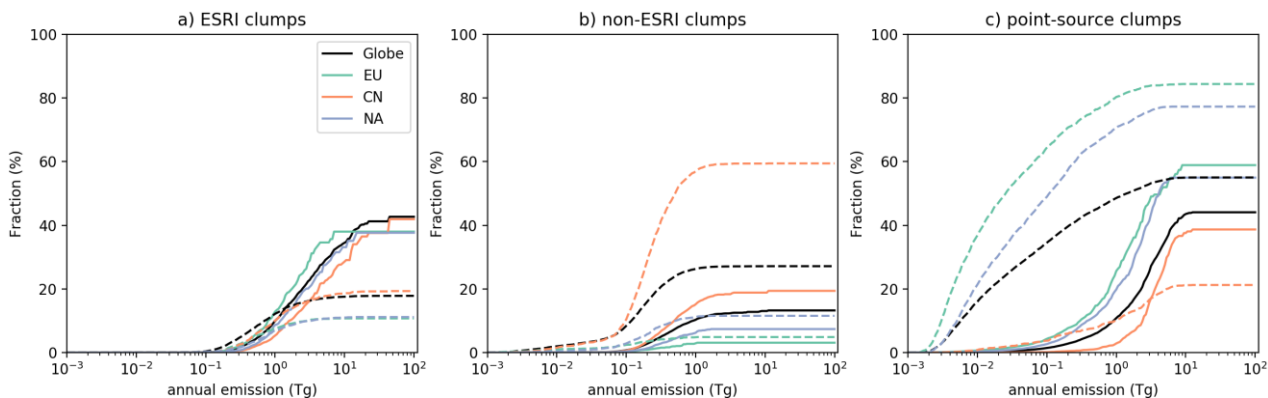


Figure 7 Cumulative distributions of the number (dashed lines) of emission clumps and of the emissions (solid lines) of the clumps for three categories of clumps (see text).

340 **Table 1** Characteristics of clumps defined in this study for the globe, European continent (European Russia included), China, North America (NA), South America (SA), Africa, Australia and Asia with China excluded (AS).

	Globe	Europe	China	NA
--	-------	--------	-------	----

Total number of clumps	11314	2470	2091	2616
Number of ESRI clumps	2017	300	404	292
Number of non-ESRI clumps	3071	243	1243	302
Number of point-source clumps	6226	1927	444	2022
Mean area of one area clump (km ²)	196	125	337	137
Maximum area of one area clump (km ²)	10356	6874	5762	5568
Mean emission budget of one clump (Tg yr ⁻¹)	0.57	0.31	1.02	0.45
Maximum emission budget of one clump (Tg yr ⁻¹)	47	17	47	15
Minimum emission budget of one clump (Tg yr ⁻¹)	9.9×10^{-4}	9.9×10^{-3}	21×10^{-4}	19×10^{-4}
Clump that has the largest annual emission	Shanghai	Moscow	Shanghai	Los Angeles
Fraction of emissions from defined clumps to total emission	72%	60%	84%	70%
Share of urban CO ₂ emissions to regional total in IEA report	67%	69%	75%	80%
Share of urban energy use to regional total in GEA report	76%	77% ¹	65% ²	86%

(Table 1 continued)

	SA	Africa	Australia	AS
Total number of clumps	477	470	110	2784
Number of ESRI-urban clumps	172	108	12	705
Number of non-ESRI clumps	69	144	5	1007
Number of point-source clumps	235	218	93	1072
Mean area of one area clump (km ²)	186	183	133	229
Maximum area of one area clump (km ²)	4303	3438	3113	10356
Mean emission budget of one clump (Tg yr ⁻¹)	0.35	0.43	0.69	0.63
Maximum emission budget of one clump (Tg yr ⁻¹)	12	11	6.8	22
Minimum emission budget of one clump (Tg yr ⁻¹)	20×10^{-4}	26×10^{-4}	21×10^{-4}	17×10^{-4}
Clump that has the largest annual emission	Buenos Aires	Johannesburg	Melbourne	Riyadh

Fraction of emissions from defined clumps to total emission	52%	62%	76%	69%
Share of urban CO ₂ emissions to regional total in IEA report	-	-	78%	-
Share of urban energy use to regional total in GEA report	85%	69% ³	78%	63% ⁴

¹ Arithmetic mean of values for Western Europe and Eastern Europe

² In GEA report, this value correspond to China and Central Pacific Asia

³ Arithmetic mean of values for Sub-Saharan Africa, North Africa and Middle East

⁴ Arithmetic mean of values for Pacific Asia and South Asia

3.2 Emission clumps based on other emission maps

The clump results obviously depend on the input emission field. The ODIAC map is chosen as a reference because it is the only global map with a spatial resolution of ~ 1 km that we are aware of. But there are other emission products with coarser resolution or having only regional coverage. To test the dependency of calculated clumps on the choice of emission map, we apply the algorithm to three alternative global emission maps and two regional emission maps (Table 2). The three global emission maps are: PKU-CO₂ v2 (Wang et al., 2013), FFDAS v2.0 (Rayner et al., 2010; Asefi-Najafabady et al., 2014), EDGAR 4.3.2 (Janssens-Maenhout et al., 2017). The two regional emission maps are: the Multi-resolution Emission Inventory (MEIC) v1.2 for China (<http://meicmodel.org/>; Zheng et al., 2018) and the VULCAN inventory (Gurney et al., 2009) v2.2 for the contiguous U.S. The resolutions of these emission maps are 0.1 °or 10 km (Table 2), that is, about 12 times coarser than ODIAC. Note that some small (in terms of area) groups of grid cells with high emission rates at a finer scale-resolution than 0.1 °are averaged at-to the coarser grid cells in these coarser-resolution maps. The clumps derived from these alternative emission maps thus have a tendency to miss small clumps, compared to ODIAC. However, the comparison of the results for the largest clumps is still indicative of the robustness of the clump definition. The years of the additional emission maps are different from the year of ODIAC (Table 2) because some institutions do not have not released their emission maps for 20167. We scale the different emission maps to the same national totals as ODIAC and we assume that the spatial distribution of clumps do not change significantly at the continental and global scales so that the differences in the year for different emission maps is not expected to have strong impacts on the clump results. We compare the fractions of emissions in alternative maps (X) covered by the clumps calculated from these map (X-clumps) with the fraction covered by ODIAC-clumps to see whether the ODIAC-clump results miss significant emissions from X. Because the resolution of ODIAC and alternative emission maps are different, when computing the X emissions covered by ODIAC-clumps, we downscale map X to 30", assuming that emissions are distributed uniformly within each 0.1 °or 10 km grid cell. Since the actual distribution of emissions within each 0.1 °or 10 km grid cell is probably not uniform, this computation tends to overestimate the differences between ODIAC-clumps and X-clumps.

Table 2 The alternative emission maps used to compare with the results of ODIAC

Emission product	Coverage	Resolution	Year	Reference
EDGAR 4.3.2	Global	0.1°×0.1 °	2010	Janssens-Maenhout et al., 2017
PKU-CO ₂ v2	Global	0.1°×0.1 °	2010	Wang et al., 2013
FFDAS v2.0	Global	0.1°×0.1 °	2009	http://hpcg.purdue.edu/FFDAS/Map.php ; Rayner et al., 2010; Asefi-Najafabady et al., 2014
MEIC v1.2	Global	0.1°×0.1 °	2010	http://meicmodel.org ; Zheng et al., 2018
VULCAN v2.2	74%	10 km×10 km	2002	Gurney et al., 2009

375

Each 30" grid cell is classified into a confusion matrix (CM) with 4 categories: 1) grid cell belongs to ODIAC-clump and X-clump (true positive, TP); 2) grid cell belongs to ODIAC-clump but not to X-clump (false positive, FP); 3) grid cell belongs to X-clump but not to ODIAC-clump (false negative, FN); and 4) grid cell neither in ODIAC-clump nor in X-clump (true negative, TN). The fractions of emissions in each CM category are computed for different regions. This comparison mainly allows us to verify whether the clumps delineated by the two thresholds are consistent using ODIAC and other maps.

380

We also checked the consistency of ESRI clumps between ODIAC-clump and X-clumps with a similar CM. Each grid cell is classified into four categories: 1) grid cell belongs to the same ESRI clump in ODIAC and X (ESRI-TP); 2) grid cell belongs to ESRI clumps in both ODIAC and X, but does not belong to the same ESRI clump (ESRI-DIFF); 3) grid cell only belongs to an ESRI clump either in ODIAC or X (ESRI-FALSE); and 4) grid cell does not belong to any ESRI clump in ODIAC nor in X (ESRI-TN). Consistency for non-ESRI clumps is not really expected because X-clumps tend to miss small clumps because of the underlying coarser-resolution maps. Consistency is not calculated for point-source clumps because not all emission products explicitly provide names for each power plant, making it difficult to determine whether the power plants from different maps within a same grid cell are the same infrastructure.

385

VULCAN is arguably the best emission map for the US, ~~for the use of the given its use of a~~ large amount of relatively accurate data from local to national scales. PKU-CO₂-v2 and MEIC v1.2, derived by Chinese institutions, used the exact locations of power plants and factories in China and detailed information of fuel consumption of each power plants and factories to estimate the point sources. They also used provincial data to distribute the non-point source emissions, resulting in more accurate estimates in the distribution of Chinese emissions than other global maps (Wang et al., 2013). EDGAR v4.3.2, developed by the Joint Research Center under the European Commission's service, has more ~~realistic-accurate~~ emission estimates in Europe. Therefore, we focus the clump consistency analysis between ODIAC and EDGAR v4.3.2 for Europe, between ODIAC, PKU-CO₂-v2 and MEIC v1.2 for China, and between ODIAC and VULCAN v2.2 for the US.

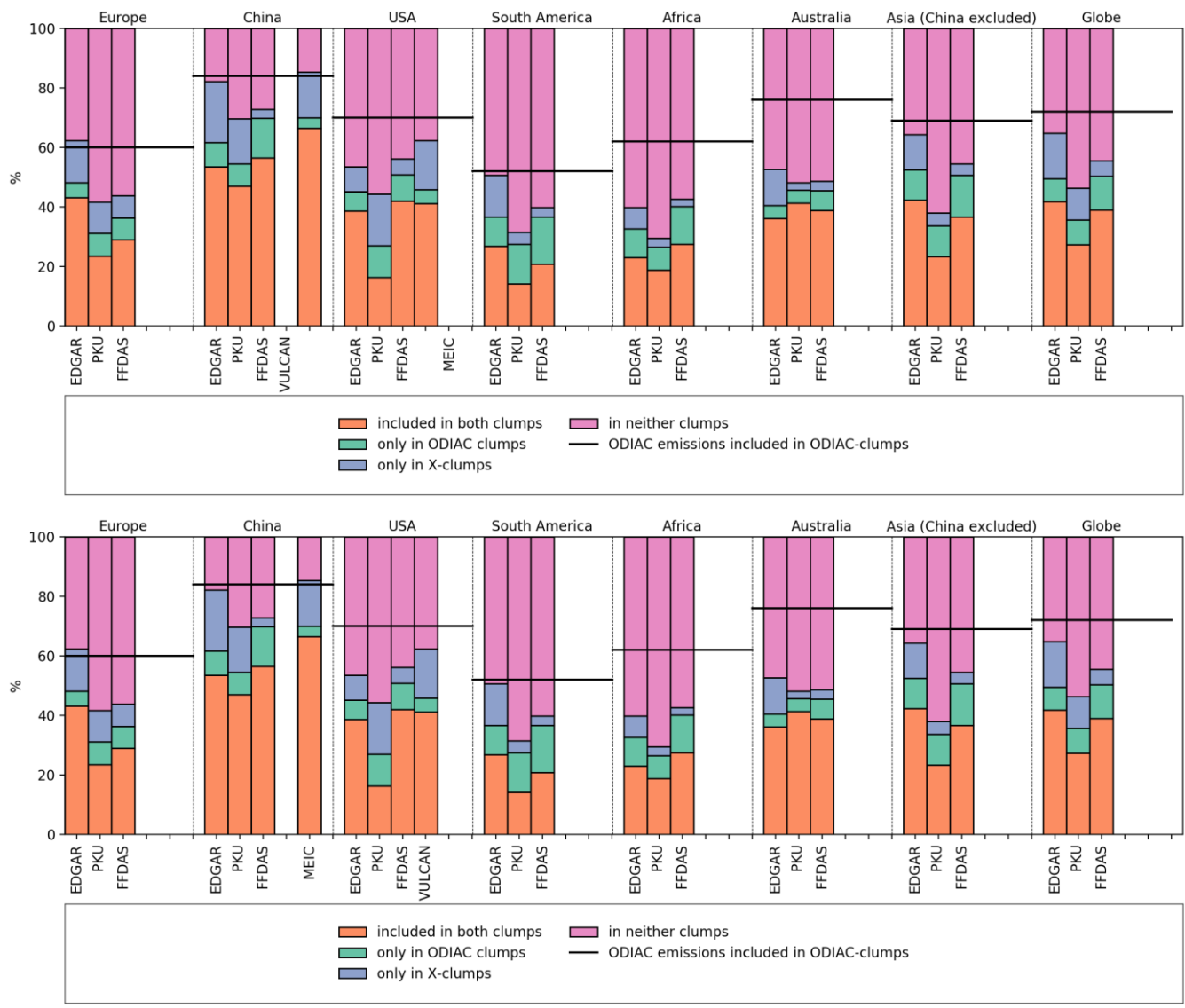
390

395

Figure 8 shows the results of the CM analysis. In general, there is a considerable fraction of national/regional emissions

covered by both ODIAC-clump and X-clump (red bars). The sum of the fractions of TP (red bars) and TN (pink bars) are larger than 70% for all countries and regions, indicating that the algorithm applied to different maps allocates consistently the same groups of emitting grid cells into clumps. In Europe, the fraction of EDGAR emissions allocated to EDGAR-clumps (red plus blue bars in Fig. 8) is close to the fraction of ODIAC emissions allocated to ODIAC clumps (black line). In China, the fraction from MEIC is also close to that derived from ODIAC. But this fraction in PKU-CO₂-v2 (54%) is lower than that derived from ODIAC in China (84%). The differences between these fractions derived from ODIAC, MEIC and PKU-CO₂-v2 indicate large uncertainties in the distribution of emissions in China. This fraction in VULCAN (46%) is lower than that derived from ODIAC in USA (73%). In addition, in all regions, the fractions of emissions allocated to X-clumps (red plus blue bars) in X emission maps are all lower than those derived from ODIAC, indicating the emissions in ODIAC are more centralized toward populated areas than in other maps. This is attributed to the lack of line sources in ODIAC (Oda et al., 2018). The blue bars in Fig. 7, representing emissions from X maps that are not covered by ODIAC-clumps, are less than 10% of the total emissions in most cases, indicating that ODIAC-clumps miss only a small fractions of emission hotspots compared to other plausible fossil fuel CO₂ emission fields even without any adjustment. However, ODIAC-clumps would capture some low-emitting grid cells in other emission maps, as shown by the green bars in Fig. 8. Further investigation into the three types of clumps: ESRI clumps, non-ESRI clumps and point-sources clumps shows that the largest differences between ODIAC and X lie in the latter two types (Fig. S1-S3). The non-ESRI clumps account for a small fraction of the total emissions (less than 20% in general, Fig. 6 and S2), and the coherence in terms of fractions of emissions covered by non-ESRI clumps between different emission maps is less than 5% (red bars in Fig. S2). There are also large disagreements in the emissions from point-source clumps between different emission maps, as displayed by Fig. S3.

Figure 9 examines the consistency of the fractions of emissions covered by the same clumps between ODIAC and any emission map X. The consistency indicated by the red and pink bars is larger than 70%. The green bars are less than 10% in general, indicating that there are not many emission grid cells connecting different large cities. The major differences between ESRI clumps derived from various emission maps come from grid cells near the borders of ESRI clumps so that they are classified as ESRI clumps or other clumps in different emission maps (blue bars).



425

Figure 8 The fractions of emissions from corresponding emission products covered: 1) by both ODIAC-clumps and X-clumps (red); 2) only by X-clumps but not by ODIAC-clumps (green); 3) by ODIAC-clumps but not by X-clumps (blue); and 4) by neither ODIAC-clumps nor X-clumps (pink). The thick black lines indicate the fractions of emissions in ODIAC covered by ODIAC-clumps.

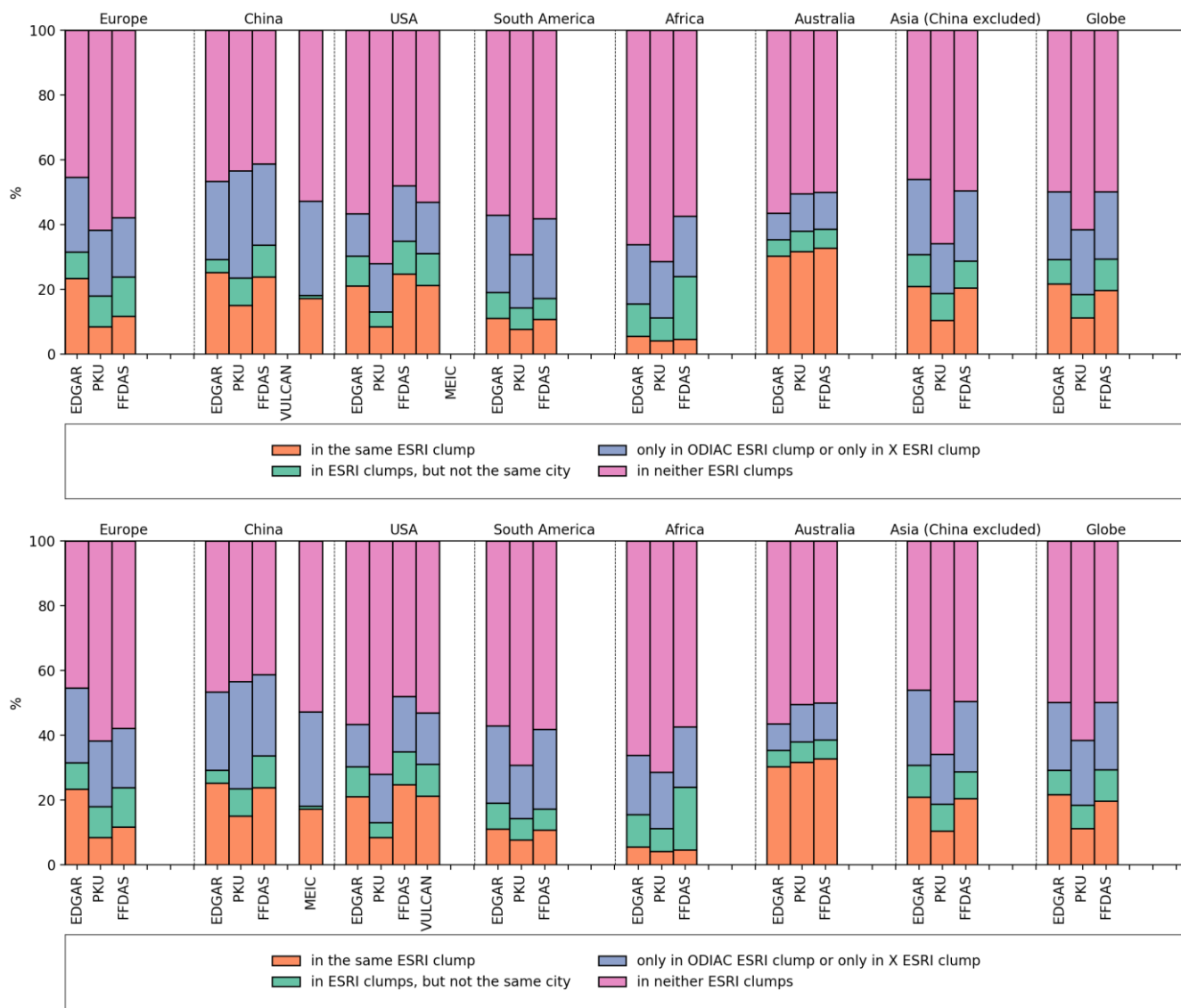


Figure 9 The fractions of emissions from corresponding emission products covered 1) by the same ESRI clump from ODIAC and X (red); 2) by ESRI clumps in both ODIAC and X, but do not belong to the same ESRI urban area (green); 3) only by one of the ESRI clump in either ODIAC or X (blue); and 4) neither by any ESRI clump in ODIAC nor in X (pink).

4. Discussion

4.1 Impacts of the sounding precision on the identification of emission clumps

In this study, we use the map of urban area from ESRI and two thresholds to derive emission clumps. Threshold-1
440 determines the cores of the clumps, corresponding to a XCO₂ enhancement larger than the precision (0.5 ppm) of individual
soundings without atmospheric horizontal transport (see Sect. 2.2 and Appendix). The precision largely depends on the designs
and configurations of different satellites. In this section, we test the sensitivity of the clumps to different assumptions on
threshold-1 related to the precision of an individual sounding. The results listed in Table 3 show that the number of clumps are
very sensitive to threshold-1, or individual XCO₂ sounding precision. However, the fractions of emissions covered by the
445 clumps do not change significantly with threshold-1. The total number of clumps is reduced by 34% when the precision of an
individual XCO₂ measurement is degraded to 1.0 ppm, compared to that obtained assuming 0.5 ppm, but the fraction of
emissions covered by all clumps is only reduced from 72% to 61%, e.g. 15% relative change. This indicates that a larger value
of threshold-1 mainly removes clumps with small emissions. On the other hand, the number and fraction of emissions covered
by point-source clumps are not sensitive to threshold-1, due to the fact that their emissions are highly concentrated in limited
450 area. On the contrary, the number and emissions associated with non-ESRI clumps are the most sensitive to the precision.

Threshold-2 is used to define which grid cells shall be aggregated with the cores to form a clump. In this study, threshold-
2 is chosen an order of magnitude smaller than threshold-1. This choice is somewhat arbitrary to include some marginal areas.
Such marginal area accounts for the fact that the outskirts of the cities could also contribute to the city cores. In addition, the
marginal area ensures that the effective clumps (e.g. the cores of the clumps) will always be accounted for in the clump map
455 within a short time span (typically within one year to among few years). With this default choice of threshold-2, the fraction
of emissions from clumps to the total emissions is occasionally close to the estimate of the share of CO₂ emissions or energy
use from cities to regional total in EIA and GEA (Table 1). The last two columns in Table 3 list the results for different values
of threshold-2. Threshold-2 mainly impacts the extent of surrounding grid cells near the cores of each area clump. When
threshold-2 is chosen to be 0.071 g C m⁻² hr⁻¹ (twice as large as the default one), keeping threshold-1 as 0.36 g C m⁻² hr⁻¹, the
460 fraction of emissions covered by the clumps to the global total is reduced from 72% (default result, T2) to 66%. The comparison
between the results of T2, T6, and T4 in Table 3 shows that the identification of non-ESRI clumps is more sensitive to
threshold-1 (precision), while the identification of ESRI clumps is more sensitive to threshold-2 (grid cells around cores in
ESRI urban areas).

465

470 **Table 3** The sensitivity of number of emission clumps (integers before parentheses) and the fractions of emissions covered by

the emission clumps (values in the parentheses) to global total to the thresholds in the clump algorithm

Experiments	T1	T2	T3	T4	T5	T6
Precision of a single sounding (ppm)	0.3 ppm	0.5 ppm	0.7 ppm	1.0 ppm	0.5 ppm	0.5 ppm
Threshold-1 (g C m ⁻² hr ⁻¹)	0.21	0.36	0.5	0.71	0.36	0.36
Threshold-2 (g C m ⁻² hr ⁻¹)	0.021	0.036	0.05	0.071	0.05	0.071
ESRI clumps	2756 (36%)	2017 (32%)	1498 (29%)	1009 (26%)	2017 (30%)	2017 (28%)
Non-ESRI clumps	6332 (15%)	3071 (10%)	1837 (7.7%)	1109 (6%)	3071 (9.2%)	3071 (8.4%)
Point-source clumps	6928 (30%)	6226 (30%)	5774 (30%)	5304 (30%)	6226 (30%)	6226 (30%)
Total	16016 (80%)	11314 (72%)	9109 (67%)	7422 (61%)	11314 (69%)	11314 (66%)

4.2 Impact of using ODIAC on the identification of emission clumps

ODIAC used nighttime light as a proxy for the spatial distribution of emissions. The accuracy of the proxy in representing the distribution of actual emissions largely impacts the extent of the clumps. For example, compared with other emission products, ODIAC does not capture line source emissions such as on-road transportation (Oda et al., 2018; Gurney et al., 2019). The satellite observations of CO indicated significant CO enhancement over major roads (Borsdorff et al., 2019). Since our clump map is derived from ODIAC emission product, some of the roads that generate significant XCO₂ plumes may be missed by the clumps defined in this study. As the ODIAC team is planning to include transportation network data in their emission product (Oda et al., 2018), our clump map could be updated with a new version of ODIAC.

~~The emission clumps is a valuable concept relevant for the monitoring of fossil fuel CO₂ emissions from satellites.~~ Fig. 8 shows that if the ODIAC-clumps are applied to other emission maps even without any adjustment, a majority of emission hotspots (indicated by red plus green bars in Fig. 8) are still included in the clump areas. However, Fig. 9 shows that there are large differences in the way emitting grid cells are grouped depending on the input emission map. When multiplying the map of ODIAC-clumps by another X emission map, the difference between the emissions from ODIAC and the emissions from the same area in the X map, for a single clump, range between 0%-165% (5th - 95th percentiles). The relative differences tend to be larger for small clumps than large ones. For the monitoring of fossil fuel CO₂ emissions from the space, these results highlight the necessity to objectively associate the observed CO₂ plumes with underlying emitting regions.

In this study, the clumps are only defined based on the ODIAC emission map for the year 2016. However, in the regions experiencing fast urbanization rates, the spatial distribution of emissions are also changing rapidly. In order to build an operational observing system in the near future, it is also necessary to consistently update the clump definition based on the latest emission maps to track the trends in the emissions and CO₂ plumes for growing cities.

4.3 Implication for future inversion studies

495 The emission clumps is a valuable concept relevant for the monitoring of fossil fuel CO₂ emissions from satellites. The
emission clumps defined in this study have at least one grid cell that will generate an excess of XCO₂ of at least 0.5 ppm over
a morning period of 6 hours, assuming no atmospheric horizontal transport. This assumption is optimistic in terms of
detectability of XCO₂ plumes. In reality, accounting for wind advection or vegetation fluxes near a clump, XCO₂ enhancement
in plumes may be smaller than 0.5 ppm, and therefore harder to detect with imagers. In this sense, the emissions covered in
500 emission clumps derived based on such an assumption conservatively define the upper fraction of fossil fuel CO₂ emissions
that could be constrained by XCO₂ imagery. In addition, the sampling of plumes will be reduced in presence of clouds, and
will suffer from XCO₂ biases related to aerosol loads (Broquet et al., 2018; Pillai et al., 2016). The emission clumps defined
in this study provide a test bed for assessing the potential of satellite imagery for monitoring fossil fuel CO₂ emissions. In the
future, global/regional inversion systems and observing system simulation experiment (OSSE) frameworks shall be developed
505 using emission fields classified into clumps. Such inversions and OSSE studies will play a critical role in the deployment of
new observation strategies and assessing the potential of these observing systems for assessing the fossil fuel CO₂ emissions
(e.g. Broquet et al., 2018; Turner et al., 2016; Pillai et al., 2016).

5. Data availability

The ODIAC2017 data product is available from a website can be downloaded from the website
510 <http://db.cger.nies.go.jp/dataset/ODIAC/> (or <https://doi.org/10.17595/20170411.001>). The TIMES data product can be
downloaded from http://cdiac.ess-dive.lbl.gov/ftp/Nassar_Emissions_Scale_Factors/. The clump map can be downloaded
from <https://doi.org/10.6084/m9.figshare.7217726.v1>.

6. Summary and Conclusion

In this study, we have identified a set of ~~large~~ emission clumps with large emission rates (in the unit of g C m⁻² hr⁻¹) from
515 a high-resolution emission inventory. These clumps will generate individual atmospheric XCO₂ plumes that may be observed
from space. This ~~method identifies~~identification method identify the clump cores using ESRI map of major urban area and a
high threshold related to the precision of XCO₂ measurements from planned satellites. It uses a low threshold and a RW
algorithm to consider the area in the vicinity of the cores and split the area between different clumps based on the spatial
gradients in the emission field. The emission clumps defined in this study depict the emitting hotspots around the globe that
520 are relevant for the monitoring of fossil fuel CO₂ emissions from the satellites measurements. The clumps are derived with a
trans-boundary approach, bypassing any artificial border imposed by national emissions accounting. In total, the emission
clumps cover 72% of the total emissions in the original ODIAC. They defines the scales and regions of monitoring the short-
term temporal profiles and long term trends in fossil fuel CO₂ emissions, which might be very useful for the Global Stocktaking

525 exercise of UNFCCC. The clumps that have been identified here span a large range of emission. Given actual atmospheric transport condition, it is not clear whether those in the low range of emission generate an atmospheric CO₂ plume that can be identified from space. The presence of cloud cover may also challenge the detection of XCO₂ plumes and thus the estimate of emissions using space-borne measurements. Which fraction of the identified clump can be observed from space, and what accuracy can be expected from the atmospheric inversion requires an OSSE framework which shall be developed in a future paper.

530 Appendix

We make a calculation of the emission flux that would generate a 0.5 ppm excess of XCO₂ during 6 hours without wind. This is a conservative case with the accumulation of all emissions in the air column. The 0.5 ppm XCO₂ is taken as the individual sounding precision of a satellite CO₂ imager. Assuming a constant emission rate F (g C m⁻² hr⁻¹) during 6 hours, the XCO₂ excess (XCO₂, unit: ppm) is given by:

$$535 \quad XCO_2 = F \times 6 / M_C / X_{air} \times 10^6 \quad (1)$$

where M_C (=12×10⁻³ kg mol⁻¹) represented the molar mass of C, X_{air} (unit: mol m⁻²) represented the molar quantity of air mass in the air column. The X_{air} could be approximated by:

$$X_{air} = P_{surf} / g / M_{air} \quad (2)$$

540 where P_{surf} (=1.013×10⁵ Pa) represents the surface pressure, g (=9.8 m s⁻²) represents the acceleration of gravity, M_{air} (=29×10⁻³ kg mol⁻¹) represents the average molar mass of air. Thus, the minimum emissions F* that would generate a 0.5 ppm excess of XCO₂ is computed: F*=0.36 g m⁻² hr⁻¹.

References

- 545 Asefi-Najafabady, S., Rayner, P. J., Gurney, K. R., McRobert, A., Song, Y., Coltin, K., Huang, J., Elvidge, C. and Baugh, K.: A multiyear, global gridded fossil fuel CO₂ emission data product: Evaluation and analysis of results, *J. Geophys. Res.*, n/a-n/a, doi:10.1002/2013jd021296, 2014.
- Boden, T. A., Marland, G. and Andres, R. J.: Global, Regional, and National Fossil-Fuel CO₂ Emissions, [online] Available from: http://cdiac.ess-dive.lbl.gov/epubs/ndp/ndp058/ndp058_v2016.html (Accessed 2 August 2018), 2016.
- 550 [Borsdorff, T., van de Brugh, J., Pandey, S., Hasekamp, O., Aben, I., Houweling, S. and Landgraf, J.: Carbon monoxide air pollution on sub-city scales and along arterial roads detected by the Tropospheric Monitoring Instrument, *Atmospheric Chemistry and Physics*, 19\(6\), 3579–3588, doi:<https://doi.org/10.5194/acp-19-3579-2019>, 2019.](#)
- Bovensmann, H., Buchwitz, M., Burrows, J. P., Reuter, M., Krings, T., Gerilowski, K., Schneising, O., Heymann, J., Tretner, A. and Erzinger, J.: A remote sensing technique for global monitoring of power plant CO₂ emissions from space and related applications, *Atmospheric Measurement Techniques*, 3(4), 781–811, 2010.
- 555 Bróń, F. M., Broquet, G., Puygrenier, V., Chevallier, F., Xueref-Remy, I., Ramonet, M., Dieudonné E., Lopez, M., Schmidt, M., Perrussel, O. and Ciais, P.: An attempt at estimating Paris area CO₂ emissions from atmospheric concentration

measurements, *Atmospheric Chemistry and Physics*, 15(4), 1707–1724, doi:10.5194/acp-15-1707-2015, 2015.

Broquet, G., Brón, F.-M., Renault, E., Buchwitz, M., Reuter, M., Bovensmann, H., Chevallier, F., Wu, L. and Ciais, P.: The potential of satellite spectro-imagery for monitoring CO₂ emissions from large cities, *Atmos. Meas. Tech.*, 11(2), 681–708, doi:10.5194/amt-11-681-2018, 2018.

Buchwitz, M., Reuter, M., Bovensmann, H., Pillai, D., Heymann, J., Schneising, O., Rozanov, V., Krings, T., Burrows, J. P., Boesch, H., Gerbig, C., Meijer, Y. and Löscher, A.: Carbon Monitoring Satellite (CarbonSat): assessment of atmospheric CO₂ and CH₄ retrieval errors by error parameterization, *Atmos. Meas. Tech.*, 6(12), 3477–3500, doi:10.5194/amt-6-3477-2013, 2013.

Cao, X., Chen, J., Imura, H. and Higashi, O.: A SVM-based method to extract urban areas from DMSP-OLS and SPOT VGT data, *Remote Sensing of Environment*, 113(10), 2205–2209, doi:10.1016/j.rse.2009.06.001, 2009.

Chatterjee, A., Gierach, M. M., Sutton, A. J., Feely, R. A., Crisp, D., Eldering, A., Gunson, M. R., O’Dell, C. W., Stephens, B. B. and Schimel, D. S.: Influence of El Niño on atmospheric CO₂ over the tropical Pacific Ocean: Findings from NASA’s OCO-2 mission, *Science*, 358(6360), eaam5776, doi:10.1126/science.aam5776, 2017. Creutzig, F., Baiocchi, G., Bierkandt, R., Pichler, P.-P. and Seto, K. C.: Global typology of urban energy use and potentials for an urbanization mitigation wedge, *PNAS*, 112(20), 6283–6288, doi:10.1073/pnas.1315545112, 2015.

Ciais, P., Crisp, D., Denier van der Gon, H. A. C., Engelen, R., Heimann, M., Janssens-Maenhout, G., Rayner, P. and Scholze, M.: Towards a European Operational Observing System to Monitor Fossil CO₂ emissions, European Commission Directorate-General for Internal Market, Industry, Entrepreneurship and SMEs Directorate I — Space Policy, Copernicus and Defence, 2015.

Doll, C. N. H. and Pachauri, S.: Estimating rural populations without access to electricity in developing countries through night-time light satellite imagery, *Energy Policy*, 38(10), 5661–5670, doi:10.1016/j.enpol.2010.05.014, 2010.

Eldering, A., Wennberg, P. O., Crisp, D., Schimel, D. S., Gunson, M. R., Chatterjee, A., Liu, J., Schwandner, F. M., Sun, Y., O’Dell, C. W., Frankenberg, C., Taylor, T., Fisher, B., Osterman, G. B., Wunch, D., Hakkarainen, J., Tamminen, J. and Weir, B.: The Orbiting Carbon Observatory-2 early science investigations of regional carbon dioxide fluxes, *Science*, 358(6360), eaam5745, doi:10.1126/science.aam5745, 2017.

Elvidge, C. D., Baugh, K. E., Kihn, E. A., Kroehl, H. W. and Davis, E. R.: Mapping city lights with nighttime data from the DMSP Operational Linescan System, *Photogrammetric Engineering and Remote Sensing*, 63(6), 727–734, 1997.

Grady, L.: Random Walks for Image Segmentation, *IEEE Transactions on Pattern Analysis and Machine Intelligence*, 28(11), 1768–1783, doi:10.1109/TPAMI.2006.233, 2006.

Grubler, A., Bai, X., Buettner, T., Dhakal, S., Fisk, D. J., Ichinose, T., Keirstead, J. E., Sammer, G., Satterthwaite, D., Schulz, N. B., Shah, N., Steinberger, J. and Weisz, H.: Chapter 18 - Urban Energy Systems, in *Global Energy Assessment - Toward a Sustainable Future*, pp. 1307–1400, Cambridge University Press, Cambridge, UK and New York, NY, USA and the International Institute for Applied Systems Analysis, Laxenburg, Austria., 2012.

Gurney, K. R., Mendoza, D. L., Zhou, Y., Fischer, M. L., Miller, C. C., Geethakumar, S. and Can, S. de la R. du: High Resolution Fossil Fuel Combustion CO₂ Emission Fluxes for the United States, *Environmental Science & Technology*, 43(14), 5535–5541, 2009.

[Gurney, K. R., Liang, J., O’Keeffe, D., Patarasuk, R., Hutchins, M., Huang, J., Rao, P. and Song, Y.: Comparison of Global Downscaled Versus Bottom-Up Fossil Fuel CO₂ Emissions at the Urban Scale in Four U.S. Urban Areas, *Journal of Geophysical Research: Atmospheres*, 0\(0\), doi:10.1029/2018JD028859, 2019.](#)

Hakkarainen, J., Ialongo, I. and Tamminen, J.: Direct space-based observations of anthropogenic CO₂ emission areas from OCO-2, *Geophys. Res. Lett.*, 43(21), 2016GL070885, doi:10.1002/2016GL070885, 2016.

Huang, X., Schneider, A. and Friedl, M. A.: Mapping sub-pixel urban expansion in China using MODIS and DMSP/OLS nighttime lights, *Remote Sensing of Environment*, 175, 92–108, doi:10.1016/j.rse.2015.12.042, 2016.

International Energy Agency (IEA): *World Energy Outlook 2008*, OECD Publishing, Paris, 2008.

Janssens-Maenhout, G., Crippa, M., Guizzardi, D., Muntean, M., Schaaf, E., Dentener, F., Bergamaschi, P., Pagliari, V., Olivier, J. G. J., Peters, J. A. H. W., Aardenne, J. A. van, Monni, S., Doering, U. and Petrescu, A. M. R.: EDGAR v4.3.2 Global Atlas of the three major Greenhouse Gas Emissions for the period 1970–2012, *Earth System Science Data Discussions*, 1–55, doi:https://doi.org/10.5194/essd-2017-79, 2017.

Lauvaux, T., Miles, N. L., Deng, A., Richardson, S. J., Cambaliza, M. O., Davis, K. J., Gaudet, B., Gurney, K. R., Huang, J.,

O’Keefe, D., Song, Y., Karion, A., Oda, T., Patarasuk, R., Razlivanov, I., Sarmiento, D., Shepson, P., Sweeney, C., Turnbull, J. and Wu, K.: High-resolution atmospheric inversion of urban CO₂ emissions during the dormant season of the Indianapolis Flux Experiment (INFLUX), *J. Geophys. Res.*, 121(10), 2015JD024473, doi:10.1002/2015JD024473, 2016.

- 610 Letu, H., Hara, M., Yagi, H., Naoki, K., Tana, G., Nishio, F. and Shuhei, O.: Estimating energy consumption from night-time DMPS/OLS imagery after correcting for saturation effects, *International Journal of Remote Sensing*, 31(16), 4443–4458, doi:10.1080/01431160903277464, 2010.
- Li, X. and Zhou, Y.: Urban mapping using DMSP/OLS stable night-time light: a review, *International Journal of Remote Sensing*, 38(21), 6030–6046, doi:10.1080/01431161.2016.1274451, 2017.
- 615 Li, X., Wang, X., Zhang, J. and Wu, L.: Allometric scaling, size distribution and pattern formation of natural cities, *Palgrave Communications*, 1, palcomms201517, doi:10.1057/palcomms.2015.17, 2015.
- Liu, X., Hu, G., Ai, B., Li, X. and Shi, Q.: A Normalized Urban Areas Composite Index (NUACI) Based on Combination of DMSP-OLS and MODIS for Mapping Impervious Surface Area, *Remote Sensing*, 7(12), 17168–17189, doi:10.3390/rs71215863, 2015.
- 620 Liu, L. and Leung, Y.: A study of urban expansion of prefectural-level cities in South China using night-time light images, *International Journal of Remote Sensing*, 36(22), 5557–5575, doi:10.1080/01431161.2015.1101650, 2015.
- Nassar, R., Hill, T. G., McLinden, C. A., Wunch, D., Jones, D. B. A. and Crisp, D.: Quantifying CO₂ Emissions From Individual Power Plants From Space, *Geophys. Res. Lett.*, 2017GL074702, doi:10.1002/2017GL074702, 2017.
- Nassar, R., Napier-Linton, L., Gurney, K. R., Andres, R. J., Oda, T., Vogel, F. R. and Deng, F.: Improving the temporal and spatial distribution of CO₂ emissions from global fossil fuel emission data sets, *J. Geophys. Res.*, 118(2), 917–933, doi:10.1029/2012jd018196, 2013.
- 625 O’Brien, D. M., Polonsky, I. N., Utembe, S. R. and Rayner, P. J.: Potential of a geostationary geoCARB mission to estimate surface emissions of CO₂, CH₄ and CO in a polluted urban environment: case study Shanghai, *Atmos. Meas. Tech.*, 9(9), 4633–4654, doi:10.5194/amt-9-4633-2016, 2016.
- 630 Oda, T. and Maksyutov, S.: A very high-resolution (1 km×1 km) global fossil fuel CO₂ emission inventory derived using a point source database and satellite observations of nighttime lights, *Atmospheric Chemistry and Physics*, 11(2), 543–556, doi:10.5194/acp-11-543-2011, 2011.
- Oda, T., Maksyutov, S. and Andres, R. J.: The Open-source Data Inventory for Anthropogenic CO₂, version 2016 (ODIAC2016): a global monthly fossil fuel CO₂ gridded emissions data product for tracer transport simulations and surface flux inversions, *Earth System Science Data*, 10(1), 87–107, doi:https://doi.org/10.5194/essd-10-87-2018, 2018.
- 635 Pillai, D., Buchwitz, M., Gerbig, C., Koch, T., Reuter, M., Bovensmann, H., Marshall, J. and Burrows, J. P.: Tracking city CO₂ emissions from space using a high-resolution inverse modelling approach: a case study for Berlin, Germany, *Atmos. Chem. Phys.*, 16(15), 9591–9610, doi:10.5194/acp-16-9591-2016, 2016.
- Polonsky, I. N., O’Brien, D. M., Kumer, J. B., O’Dell, C. W. and others: Performance of a geostationary mission, geoCARB, to measure CO₂, CH₄ and CO column-averaged concentrations, *Atmospheric Measurement Techniques*, 7(4), 959–981, 2014.
- 640 Rayner, P. J., Raupach, M. R., Paget, M., Peylin, P. and Koffi, E.: A new global gridded data set of CO₂ emissions from fossil fuel combustion: Methodology and evaluation, *J. Geophys. Res.*, 115, doi:10.1029/2009jd013439, 2010.
- Seto, K. C., Dhakal, S., Bigio, A., Blanco, H., Delgado, G. C., Dewar, D., Huang, L., Inaba, A., Kansal, A. and Lwasa, S.: Human settlements, infrastructure and spatial planning, in *Climate Change 2014: Mitigation of Climate Change: Contribution of Working Group III to the Fifth Assessment Report of the Intergovernmental Panel on Climate Change*, p. Chap 12, pp 923–1000, IPCC, Geneva, Switzerland., 2014.
- 645 Shan, Y., Guan, D., Hubacek, K., Zheng, B., Davis, S. J., Jia, L., Liu, J., Liu, Z., Fromer, N., Mi, Z., Meng, J., Deng, X., Li, Y., Lin, J., Schroeder, H., Weisz, H. and Schellnhuber, H. J.: City-level climate change mitigation in China, *Science Advances*, 4(6), eaaq0390, doi:10.1126/sciadv.aaq0390, 2018.
- 650 Stauffer, J., Broquet, G., Brón, F.-M., Puygrenier, V., Chevallier, F., Xueref-Rény, I., Dieudonné, E., Lopez, M., Schmidt, M., Ramonet, M., Perrussel, O., Lac, C., Wu, L. and Ciais, P.: The first 1-year-long estimate of the Paris region fossil fuel CO₂ emissions based on atmospheric inversion, *Atmos. Chem. Phys.*, 16(22), 14703–14726, doi:10.5194/acp-16-14703-2016, 2016. Tong, D., Zhang, Q., Davis, S. J., Liu, F., Zheng, B., Geng, G., Xue, T., Li, M., Hong, C. and Lu, Z.: Targeted

- 655 emission reductions from global super-polluting power plant units, *Nature Sustainability*, 1(1), 59, 2018.
- Su, Y., Chen, X., Wang, C., Zhang, H., Liao, J., Ye, Y. and Wang, C.: A new method for extracting built-up urban areas using DMSP-OLS nighttime stable lights: a case study in the Pearl River Delta, southern China, *GIScience & Remote Sensing*, 52(2), 218–238, doi:10.1080/15481603.2015.1007778, 2015.
- 660 Turner, A. J., Shusterman, A. A., McDonald, B. C., Teige, V., Harley, R. A. and Cohen, R. C.: Network design for quantifying urban CO₂ emissions: assessing trade-offs between precision and network density, *Atmos. Chem. Phys.*, 16(21), 13465–13475, doi:10.5194/acp-16-13465-2016, 2016.
- United Nations Framework Convention on Climate Change (UNFCCC): Adoption of the Paris agreement, Paris, 2015.
- Wang, Q., Wu, S., Zeng, Y. and Wu, B.: Exploring the relationship between urbanization, energy consumption, and CO₂ emissions in different provinces of China, *Renewable and Sustainable Energy Reviews*, 54, 1563–1579, doi:10.1016/j.rser.2015.10.090, 2016.
- 665 Wang, R., Tao, S., Ciais, P., Shen, H. Z., Huang, Y., Chen, H., Shen, G. F., Wang, B., Li, W., Zhang, Y. Y., Lu, Y., Zhu, D., Chen, Y. C., Liu, X. P., Wang, W. T., Wang, X. L., Liu, W. X., Li, B. G. and Piao, S. L.: High-resolution mapping of combustion processes and implications for CO₂ emissions, *Atmospheric Chemistry and Physics*, 13(10), 5189–5203, doi:10.5194/acp-13-5189-2013, 2013.
- 670 Zheng, B., Tong, D., Li, M., Liu, F., Hong, C., Geng, G., Li, H., Li, X., Peng, L., Qi, J., Yan, L., Zhang, Y., Zhao, H., Zheng, Y., He, K. and Zhang, Q.: Trends in China's anthropogenic emissions since 2010 as the consequence of clean air actions, *Atmospheric Chemistry and Physics*, 18(19), 14095–14111, doi:https://doi.org/10.5194/acp-18-14095-2018, 2018.
- Zhou, Y., Smith, S. J., Zhao, K., Imhoff, M., Thomson, A., Bond-Lamberty, B., Asrar, G. R., Zhang, X., He, C. and Elvidge, C. D.: A global map of urban extent from nightlights, *Environ. Res. Lett.*, 10(5), 054011, doi:10.1088/1748-9326/10/5/054011, 2015.
- 675 Zhou, Y., Smith, S. J., Elvidge, C. D., Zhao, K., Thomson, A. and Imhoff, M.: A cluster-based method to map urban area from DMSP/OLS nightlights, *Remote Sensing of Environment*, 147, 173–185, 2014.